

1 **Full title**

2  
3 **Short-range interactions between fibrocytes and CD8<sup>+</sup> T cells in COPD bronchial**  
4 **inflammatory response**  
5  
6  
7

8 **Authors**

9 Edmée Eyraud<sup>1,2</sup>, Elise Maurat<sup>1,2</sup>, Jean-Marc Sac-Epée<sup>3</sup>, Pauline Henrot<sup>1,2,4</sup>, Maeva  
10 Zysman<sup>1,2,4</sup>, Pauline Esteves<sup>1,2</sup>, Thomas Trian<sup>1,2</sup>, Hugues Bégueret<sup>1,2,4</sup>, Pierre-Oliver  
11 Girodet<sup>1,2,4</sup>, Matthieu Thumerel<sup>1,2,4</sup>, Romain Hustache-Castaing<sup>1,2,4</sup>, Roger  
12 Marthan<sup>1,2,4</sup>, Florian Levet<sup>5,6</sup>, Pierre Vallois<sup>3</sup>, Cécile Contin-Bordes<sup>7,8</sup>, Patrick  
13 Berger<sup>1,2,4</sup>, Isabelle Dupin<sup>1,2,\*</sup>  
14

15 **Affiliations**

16  
17 <sup>1</sup>Univ-Bordeaux, Centre de Recherche Cardio-thoracique de Bordeaux, U1045,  
18 Département de Pharmacologie, CIC1401, Pessac, France. <sup>2</sup>INSERM, Centre de  
19 Recherche Cardio-thoracique de Bordeaux, U1045, CIC1401, Pessac, France.  
20 <sup>3</sup>Univ-Lorraine, Institut Elie Cartan de Lorraine, UMR7502, Vandoeuvre-lès-  
21 Nancy, France. <sup>4</sup>CHU de Bordeaux, Service d'exploration fonctionnelle respiratoire,  
22 CIC1401, Pessac, France. <sup>5</sup>Univ. Bordeaux, CNRS, Interdisciplinary Institute for  
23 Neuroscience, IINS, UMR 5297, Bordeaux, France. <sup>6</sup>Univ. Bordeaux, CNRS,  
24 INSERM, Bordeaux Imaging Center, BIC, UAR3420, US 4, Bordeaux, France.  
25 <sup>7</sup>CNRS, UMR5164 ImmunoConcEpT, Université de Bordeaux, Bordeaux, France.  
26 <sup>8</sup>CHU de Bordeaux, Laboratoire d'Immunologie et Immunogénétique, Bordeaux,  
27 France  
28  
29

30 **\* Corresponding author:** Pr Isabelle DUPIN, PhD

31 Centre de recherche Cardio-thoracique de Bordeaux INSERM U1045

32 PTIB - Hôpital Xavier Arnoz, Avenue du Haut Lévêque, 33600 PESSAC

33 e-mail: [isabelle.dupin@u-bordeaux.fr](mailto:isabelle.dupin@u-bordeaux.fr)

34 **Abstract**

35 The peri-bronchial zone of chronic obstructive pulmonary disease (COPD) is the site of  
36 extensive infiltration of immune cell, allowing persistent contacts between resident cells  
37 and immune cells. Tissue fibrocytes interaction with CD8<sup>+</sup> T cells and its consequences  
38 were investigated. We show that fibrocytes and CD8<sup>+</sup> T cells are found in vicinity in distal  
39 airways and that potential interactions are more frequent in tissues from COPD patients  
40 compared to those of control subjects. Increased proximity and clusterization between  
41 CD8<sup>+</sup> T cells and fibrocytes are associated with altered lung function. Tissular CD8<sup>+</sup> T cells  
42 from COPD patients promote fibrocyte chemotaxis via the CXCL8-CXCR1/2 axis. CD8<sup>+</sup> T  
43 cells establish short-term interactions with fibrocytes, that trigger CD8<sup>+</sup> T cell proliferation  
44 in a CD54<sup>-</sup> and CD86-dependent manner, as well as pro-inflammatory cytokines  
45 production. We defined a computational model, with intercellular interactions fitting to  
46 our experimental measurements. This model allowed not only to accurately predicts  
47 histological ex vivo characteristics but also to monitors disease evolution. Altogether, our  
48 study reveals that local interactions between fibrocytes and CD8<sup>+</sup> T cells can occur in vivo  
49 and could jeopardize the balance between protective immunity and chronic inflammation in  
50 bronchi of COPD patients.

## 51 **Introduction**

52 The prevalence of COPD, one of the most common chronic diseases worldwide, has been  
53 rising in recent decades (Mannino & Buist, 2007); thus, prevention and treatment of COPD  
54 are important issues of global healthcare. COPD bronchi are an area of intense  
55 immunological activity and tissue remodeling, as evidenced by the extensive immune cell  
56 infiltration and changes in tissue structures such as peribronchial fibrosis. In particular,  
57 distal airways are hypothesized to constitute a “quiet zone”, where exaggerated remodeling  
58 and inflammatory processes take place early in the history of the disease, without  
59 identifiable symptoms or lung function tests alteration (Hogg et al., 1970; Mead, 1970). In  
60 these particular areas, persistent contacts occur between resident cells and stimulated  
61 immune cells migrating from the peripheral circulation to the distal airways. The relevance  
62 of direct contact between T cells and monocyte-macrophages to potentiate the inflammatory  
63 response has been demonstrated in many chronic inflammatory diseases affecting the  
64 central nervous system, osteoarticular structures and the lungs (Dayer, 2003), but remains  
65 to be fully investigated in COPD.

66 Fibrocytes, fibroblast-like leukocytes, produced by the bone marrow and released in the  
67 peripheral circulation (Bucala et al., 1994), have been implicated in lung fibrosis (Pilling et  
68 al., 2014). They are also recruited in the blood of COPD patients during an acute  
69 exacerbation (Dupin et al., 2016). High circulating fibrocyte count during a COPD  
70 exacerbation is associated with an increased risk of death, suggesting that fibrocytes could  
71 be detrimental to the evolution of this disease (Dupin et al., 2016). We have also  
72 demonstrated that tissue fibrocytes density increases in COPD bronchi, which was  
73 associated with a degraded lung function, increased wall thickness and air trapping (Dupin  
74 et al., 2019). However, the function of these fibrocytes in COPD lungs is not yet fully  
75 understood (Dupin et al., 2018). Besides their role in tissue scarring matrix production

76 (Bucala et al., 1994) and contraction (Henrot et al., 2022), recruited fibrocytes may  
77 participate to lung inflammation in virtue of their immune properties. They can function as  
78 antigen-presenting cells with T cells (Chesney et al., 1997), which can in turn modulate  
79 fibrocyte differentiation (Niedermeier et al., 2009). Fibrocyte engagement into  
80 immunomodulation has been implicated in various diseases such as thyroid-associated  
81 ophthalmopathy (Fernando et al., 2012) and lung cancer (Afroj et al., 2021). Cytotoxic  
82 CD8<sup>+</sup> T cells are predominant in the airways of COPD patients and their number inversely  
83 correlates with lung function (O'Shaughnessy et al., 1997). CD8<sup>+</sup> T cell-deficient mice are  
84 protected against lung inflammation and emphysema induced by cigarette smoke exposure  
85 (Maeno et al., 2007) whereas the expression of molecules linked to tissue destruction, such  
86 as perforin, granzyme B and ADAM15, correlate with disease severity (Freeman et al.,  
87 2010; Wang et al., 2020), suggesting CD8<sup>+</sup> T cells implication in lung inflammation and  
88 destruction in COPD. Activation of CD8<sup>+</sup> T cells is increased in COPD lung samples (Roos-  
89 Engstrand et al., 2009). Other studies have shown that CD8<sup>+</sup> T cell activation could be  
90 partially T Cell Receptor (TCR)-independent (Freeman et al., 2010). The absence of  
91 increased expression of cytotoxic enzyme in peripheral blood CD8<sup>+</sup> T cells from COPD  
92 patients argues in favor of a local activation within the lungs (Morissette et al., 2007). CD8<sup>+</sup>  
93 T cells express an exhausted phenotype in the COPD lung, that may result from an over-  
94 activation thus participating to the defective response to infection in COPD (McKendry et  
95 al., 2016). However, CD8<sup>+</sup> T cells activation's mechanism as well as their precise  
96 contribution to COPD pathogenesis remain largely unknown.

97 A recent study showed that fibrocytes, derived from the blood of lung adenocarcinoma  
98 patients, could strongly enhance the proliferation of CD8<sup>+</sup> T cells (Afroj et al., 2021). We  
99 thus hypothesized that CD8<sup>+</sup> T cells and fibrocytes interact into the lungs, and that this  
100 interaction is critical in COPD pathology. Multiple immunostainings in combination with

101 specific image analysis methods allow to determine the spatial distribution of individual  
102 CD8<sup>+</sup> T cells and fibrocytes within bronchial tissues of both control subjects and COPD  
103 patients. Using *in vitro* fibrocyte and CD8<sup>+</sup> T cell-based experiments, we studied cell  
104 interplay in terms of relative chemotaxis, dynamics, proliferation and cytokine secretion  
105 profile. We then integrated these findings into an agent-based computational model  
106 representing airways from either healthy or COPD patients enabling to test how local  
107 interactions shape spatial distributions of cell in both conditions. We propose that slight  
108 dysregulations of intercellular interactions induce abnormal cell organization around  
109 bronchi, ultimately causing a breakdown of tissue homeostasis, leading to chronic  
110 inflammation and tissue remodeling.

## 111 Results

### 112 **Direct contacts between fibrocytes and CD8<sup>+</sup> T cells are more frequent in distal** 113 **bronchial tissue from COPD patients than in that of controls**

114 We used immunohistochemistry (IHC) to assess whether fibrocytes and CD8<sup>+</sup> T cells were  
115 in close vicinity in human tissue. Sections of distal lung tissues from 17 COPD and 25  
116 control patients were obtained, from a previously described cohort (Dupin et al., 2019), and  
117 labeled to detect CD8<sup>+</sup> T cells, identified as cells positive for CD8 staining and fibrocytes,  
118 identified as cells dual positive for FSP1 and CD45 double staining (Figure S1A-D). In  
119 agreement with previous studies (Dupin et al., 2019; O’Shaughnessy et al., 1997; Saetta et  
120 al., 1998), the density of both CD8<sup>+</sup> T cells and fibrocytes was increased within the  
121 subepithelial area of distal bronchi from COPD patients compared with that of control  
122 subjects (Figure 1A-C). Moreover, fibrocytes and CD8<sup>+</sup> T cells were frequently in close  
123 proximity (Figure 1D). To quantify the potential for cell–cell contacts, we determined the  
124 density of CD8<sup>+</sup> T cells in interaction with CD45<sup>+</sup> FSP1<sup>+</sup> cells (Figure S1A-D). Whatever  
125 the magnification used to automatically count interacting cells, the density of CD8<sup>+</sup> T cells  
126 in interaction with fibrocytes was higher in the sub-epithelial region of distal bronchi of  
127 COPD patients than in that of control subjects (Figure 1D-F). For subsequent analyses, we  
128 chose the dilatation size “D8” (3.6 μm, which represents the radius of a mean ideal round  
129 cell in our analysis) to reflect the density of interacting cells. To evaluate the minimal  
130 distance between CD45<sup>+</sup> FSP1<sup>+</sup> cells and neighboring CD8<sup>+</sup> T cells, we used a CD8 distance  
131 map generated from the CD8 staining image, with the brightness of each pixel reflecting the  
132 distance from a CD8<sup>+</sup> T cell (Figure S1E-F). The mean minimal distance between fibrocytes  
133 and CD8<sup>+</sup> cells was significantly smaller in the sub-epithelial region of distal bronchi of  
134 COPD patients than in that of control subjects (Figure 1G-H). In contrast, the mean minimal  
135 distances between CD8<sup>+</sup> T cells themselves or between fibrocytes themselves were

136 unchanged (Figure S2A-B). The majority of both CD8<sup>+</sup> T cells and fibrocytes was located  
137 beneath the epithelium, with their minimal distance and distribution relatively to the basal  
138 membrane being similar in control and COPD patients (Figure S2C-F). Altogether, no  
139 difference of spatial repartition was observed within each cell population between control  
140 and COPD patients, but the relative distribution of fibrocytes and CD8<sup>+</sup> cells was affected  
141 in tissues from patients with COPD.

142 To further describe the relative spatial organization of both cell types, we used a method  
143 based on Delaunay triangulation computed on previously segmented cell barycenters. It is  
144 based on a custom developed plugin to determine congregations of small groups of cells,  
145 called “clusters” (Figure S3). As expected from our minimal distance analysis, we found  
146 difference neither in the density of single cell-type clusters nor in their size, measured by  
147 the mean number of cells by cluster, between control subjects and patients with COPD  
148 (Figure 1I-J, left and middle panels). However, the density of clusters containing both cell  
149 types (“mixed cell clusters”) was higher in distal bronchi of COPD patients than in those of  
150 control subjects, with a median number of 5 and 6 cells in these clusters in control and  
151 COPD tissues, respectively (Figure 1I-J, right panels). This result indicates that fibrocytes  
152 and CD8<sup>+</sup> T cells are found within close proximity in the peribronchial area of COPD  
153 patients, with possible co-organization of CD8<sup>+</sup> T cells and fibrocytes in mixed cell clusters,  
154 indicating that direct and/or indirect fibrocyte-CD8<sup>+</sup> T cell interactions might occur *in vivo*.

### 155 156 **Relationships between the density of CD8<sup>+</sup> T cells interacting with fibrocytes and** 157 **functional parameters**

158 We determined the univariate correlation coefficients between fibrocyte density, CD8<sup>+</sup> T  
159 cell density, the 3 variables quantifying the interaction of CD8<sup>+</sup> T cells with fibrocytes (the  
160 interacting cell density, the mean minimal distance between fibrocytes and CD8<sup>+</sup> T cells

161 and the density of mixed cell clusters), and various functional and CT parameters (Tables  
162 S1 to S5). In particular, moderate but significant univariate correlations were found between  
163 the Forced Expiratory Volume in 1 second / Forced Vital Capacity (FEV<sub>1</sub>/FVC) ratio (used  
164 to diagnose COPD if below 0.7) and the density of fibrocytes, the density of interacting  
165 cells, the mean minimal distance between fibrocytes and CD8<sup>+</sup> T cells and the density of  
166 fibrocytes-CD8<sup>+</sup> T cells clusters (Figure S4A-D). Variables significantly correlated with  
167 FEV<sub>1</sub>/FVC were entered into stepwise regression analyses in order to find the best model  
168 fitting FEV<sub>1</sub>/FVC. The best model associated the density of interacting cells and the density  
169 of mixed cell clusters. It explained 35% of the FEV<sub>1</sub>/FVC variability (Table S6). The  
170 relationships between the FEV<sub>1</sub>/FVC ratio, the density of interacting cells and the density  
171 of mixed cell clusters were all statistically significant.

### 172 **Chemo-attraction of CD8<sup>+</sup> T cells for fibrocytes is increased in COPD tissue**

174 To decipher the molecular mechanisms underpinning the increased cell-cell interaction in  
175 COPD bronchi, we investigated cell adhesion and chemotaxis processes in CD8<sup>+</sup> T cells of  
176 patients with COPD compared with those of controls. Using the transcriptomic profile of  
177 tissular resident memory and effector memory CD8<sup>+</sup> T cells of COPD patients compared  
178 with that of control subjects in the GSE61397 microarray dataset  
179 (<http://www.ncbi.nlm.nih.gov/geo/>) published elsewhere (Hombrink et al., 2016), we noted  
180 significative changes in the abundance of transcripts of genes related to cell adhesion.  
181 However, the changes were not consistent with clear increased or decreased adhesive  
182 properties in both tissue resident memory CD8<sup>+</sup> CD103<sup>+</sup> T-cells (T<sub>RM</sub>) and effector memory  
183 CD8<sup>+</sup> CD103<sup>-</sup> T-cells (T<sub>EM</sub>) (Figure S5). In contrast, transcriptomic data reveal consistent  
184 changes in COPD cells *versus* controls, mostly increases, in chemokines and chemokine  
185 receptors (Figure 2A). Most changes in transcripts were compatible with a pro-attractive



186 and a pro-migratory response. In particular, there were increases of CCL2, CCL26, CXCL2  
187 and CXCL8 expression in T<sub>RM</sub> from patients with COPD, and CCL3L1 expression in T<sub>EM</sub>  
188 from patients with COPD (Figure 2A).

189 We then investigated whether tissular CD8<sup>+</sup> T cells secretion from control or COPD patients  
190 could affect fibrocytes migration in an *in vitro* assay (Figure 2B). CD8<sup>+</sup> T cells were purified  
191 from lung resection material sampled either in control subjects or in COPD patients, whose  
192 characteristics are reported (Table S7). Precursors of fibrocytes were purified from blood  
193 samples of a separate cohort of COPD patients (*i.e.*, COBRA), whose characteristics are  
194 also reported (Table S8). The migration of fibrocytes was significantly increased by  
195 conditioned medium derived from tissular CD8<sup>+</sup> T cells of COPD patients compared with  
196 those from control lungs (Figure 2C).

197 The secretory profile of these tissular CD8<sup>+</sup> T cells 36h after culture conditions with soluble  
198 anti-CD3 and anti-CD28 antibodies was determined. The concentration of CXCL8 was  
199 increased in CD8<sup>+</sup> T cells from COPD patients compared to control cells (Figure 2D) in  
200 good agreement with the transcriptomic analysis. By contrast, the concentration of both  
201 CCL3 and CCL3L1 was undetectable (data not shown), whereas that of CCL2 and CXCL2  
202 remained unchanged (Figure 2D). Since CXCL8 is a ligand of the chemokine receptors  
203 CXCR1 and/or CXCR2, we repeated the migration assay with the addition of the drug  
204 reparixin, an antagonist of both CXCR1 and CXCR2 (Bertini et al., 2004). Whereas  
205 fibrocyte treatment with reparixin had no significant effect on the control CD8<sup>+</sup> T cells-  
206 mediated migration, it did inhibit the increased migration induced by the secretions of CD8<sup>+</sup>  
207 T cells purified from COPD tissues (Figure 2E). Moreover, an anti-CXCL8 blocking  
208 antibody also inhibited the increased migration induced by the secretions of CD8<sup>+</sup> T cells  
209 purified from COPD tissues (Figure 2F). These data indicate that tissular CD8<sup>+</sup> T cells from  
210 patients with COPD promote fibrocyte chemotaxis via CXCL8-CXCR1/2 axis.

211  
212  
213  
214  
215  
216  
217  
218  
219  
220  
221  
222  
223  
224  
225  
226  
227  
228  
229  
230  
231  
232  
233  
234  
235

### **CD8<sup>+</sup> T cells repeatedly interact with fibrocytes**

As fibrocytes and CD8<sup>+</sup> T cells reside in close proximity in the subepithelial area, especially that of tissues from COPD patients, we investigated their crosstalk capacity. We developed an autologous *in vitro* co-culture system allowing precise control over the cell types involved. Fibrocytes and CD8<sup>+</sup> T cells, both purified from blood of COPD patients were co-cultured 2 days before image acquisition for the following 12h. CD8<sup>+</sup> T cells were either nonactivated or activated with anti-CD3/CD28 antibodies coated microbeads. At the beginning of live imaging, nonactivated CD8<sup>+</sup> T cells were equally allocated in fibrocyte-covered zones ( $41 \pm 8\%$ ) and in fibrocyte-free zones ( $59\% \pm 8\%$ ) (Figure 3A-B). Twelve h later, most ( $77 \pm 9\%$ ) of CD8<sup>+</sup> T cells were present in contact with fibrocytes (Figure 3A-B). Activation of CD8<sup>+</sup> T cells resulted in similar distribution (Figure 3A-B). These data suggest that both cell types are able to directly interact, and that these interactions progressively increase during co-culture. We tracked individual CD8<sup>+</sup> T cells during 12h time lapse to capture their spatiotemporal dynamics using multiple variables quantification (Figure 3C and Movie S1). For both nonactivated and activated lymphocytes, the mean speed of CD8<sup>+</sup> T cells decreased upon contact with fibrocytes (Figure 3D). Irrespective of the activation state of CD8<sup>+</sup> T cells, a majority of intercellular contacts ( $49 \pm 6\%$  and  $49 \pm 8\%$  for nonactivated and activated CD8<sup>+</sup> T cells, respectively) were short-lived (<12 min) and dynamic, although some longer interactions (>32 min) could also be detected ( $30 \pm 4\%$  and  $27 \pm 7\%$  for nonactivated and activated CD8<sup>+</sup> T cells, respectively) (Figure 3E). The contact coefficient and the mean velocity of CD8<sup>+</sup> T cells measured in the absence of contact with fibrocytes (“Mean free speed”) were similar in both conditions of activation (Figure 3F-G). However, we observed a significant decrease in the mean speed for activated CD8<sup>+</sup> T cells when they were in contact with fibrocytes (“Mean contact speed”) compared to

236 nonactivated CD8<sup>+</sup> T cells (Figure 3H), reflecting subtle behavior changes in this condition  
237 of activation.

238

### 239 **Fibrocytes favor CD8<sup>+</sup> T cell proliferation in a cell-cell contact-dependent manner**

240 Since multiple transient contacts have been shown to be an early trigger of events leading  
241 to clonal expansion (Obst, 2015), we wondered whether fibrocytes could promote CD8<sup>+</sup> T  
242 cells proliferation using total cell count and a CellTrace-based co-culture proliferation  
243 assay. We designed two different co-culture assays modeling either a direct contact between  
244 the two cell types or an indirect contact (transwell assay). The activation of CD8<sup>+</sup> T cells by  
245 anti-CD3/CD28 antibody coated microbeads slightly increased the basal level of dividing  
246 CD8<sup>+</sup> T cells (comparison of the conditions “CD8<sub>NA</sub>” and “CD8<sub>A</sub>” without fibrocytes in  
247 Figure 3I-P). The presence of fibrocytes in the indirect co-culture assay did not affect  
248 proliferation capacity of non-activated CD8<sup>+</sup> T cells and only moderately increased the  
249 number of dividing activated CD8<sup>+</sup> T cells (Figure 3 I-L). The distinction between naïve  
250 (CD45RA<sup>+</sup>) and memory (CD45RA<sup>-</sup>) CD8<sup>+</sup> T cells did not reveal any selective effect of  
251 fibrocytes on these two CD8<sup>+</sup> subpopulations (Figure S6A, C and S6E-H). In the direct co-  
252 culture model, the total number of CD8<sup>+</sup> T cells and the percentage of dividing CD8<sup>+</sup> T cells  
253 were far higher in the presence of fibrocytes irrespective of the activation state of CD8<sup>+</sup> T  
254 cells (Figure 3M-P). This effect seemed to be particularly impressive for naïve CD8<sup>+</sup> T cells  
255 as they demonstrated an average differential of  $80 \pm 14\%$  and  $70 \pm 20\%$  of dividing cells  
256 between the conditions with and without fibrocytes, respectively for nonactivated (Figure  
257 S6I-J, top panels) and activated CD8<sup>+</sup> T cells (Figure S6I-J, bottom panels), vs  $67 \pm 18\%$   
258 and  $52 \pm 20\%$  for memory CD8<sup>+</sup> T cells (Figure S6K-L). Altogether, this implies that a  
259 direct rather than indirect interactions between CD8<sup>+</sup> T cells and fibrocytes increased CD8<sup>+</sup>  
260 T cell proliferation.

261 After 6 days of co-culture, a cell population with a low level of CD8 expression (CD8<sup>low</sup>)  
262 appeared, that was inversely proportional to the level of CD8<sup>+</sup> T cells strongly expressing a  
263 high level of CD8 (CD8<sup>high</sup>, Figure S7). The CellTrace-based assay showed that those cells  
264 highly proliferated during co-culture, especially in the direct co-culture (Figure S7E),  
265 suggesting that CD8<sup>high</sup> cells disappeared in favor of CD8<sup>low</sup> cells. As fibrocytes could have  
266 contaminated the cell suspension harvested from the direct co-culture, we did check that  
267 those CD8<sup>low</sup> cells were not CD45<sup>+</sup> Collagen I<sup>+</sup> (Figure S8). Phenotypic analysis of this  
268 CD8<sup>low</sup> population indicated that cells were mostly CD45RA<sup>-</sup> cells (Figure S7A-B, S7D-E),  
269 with a low level of cytokine expression (Figure S7C, F). Since CD8<sup>low</sup> cells may thus  
270 represent a population of exhausted T cells, we focused on CD8<sup>high</sup> cells in the following,  
271 especially regarding the secretion profile characterization. As CD86 and CD54 co-  
272 stimulatory molecule and adhesion molecule, respectively, pivotal in immunological  
273 synapse formation, are both expressed by fibrocytes (Afroj et al., 2021; Balmelli et al.,  
274 2005), we tested the effects of anti-CD54 and anti-CD86 blocking antibodies on fibrocyte-  
275 induced proliferation of CD8<sup>+</sup> T cells. The inhibition of CD86 and CD54 significantly  
276 reduced proliferation of nonactivated CD8<sup>+</sup> T cells in the direct co-culture with fibrocytes  
277 (Figure 4). However, these antibodies failed to alter the stimulatory activity of lymphocyte  
278 division by fibrocytes, when CD8<sup>+</sup> T cells were previously activated (Figure 4). Blocking  
279 LFA-1 did not affect the fibrocyte-mediated CD8<sup>+</sup> T cell division (Figure S9A-D),  
280 suggesting the existence of compensatory integrins at the surface of the lymphocyte, such  
281 as CD11b/CD18, to mediate the interaction with CD54. The inhibition of CD44, a receptor  
282 for hyaluronan which has been shown to be produced by fibrocytes (Bianchetti et al., 2012),  
283 did not impair the proliferation of CD8<sup>+</sup> T cells irrespective of their activation state (Figure  
284 S9E-H).

285 In total, these results indicate that direct contacts between fibrocytes and CD8<sup>+</sup> T cells, such  
286 as those mediated by CD54 and CD86, were strong positive signals to trigger CD8<sup>+</sup> T cell  
287 proliferation with the induction of CD8<sup>high</sup> and CD8<sup>low</sup> phenotypes.

### 289 **Fibrocyte-CD8<sup>+</sup> T cell interactions alter cytokine production**

290 Multiparametric flow cytometry was used to characterize the cytokine expression profile of  
291 CD8<sup>+</sup> T cells in the indirect and direct co-culture with fibrocytes. When nonactivated CD8<sup>+</sup>  
292 T cells were indirect co-cultured with fibrocytes, the expression of TNF- $\alpha$ , IFN- $\gamma$  by CD8<sup>+</sup>  
293 T cells was slightly increased (Figure 5A-B). IL-10, IL-17 and Granzyme B were not  
294 detected (Figure 5A-B). When CD8<sup>+</sup> T cells were activated with anti-CD3/CD28, the level  
295 of TNF- $\alpha$  and IFN- $\gamma$  further increased, and the expression of granzyme B and IL-10 was  
296 slightly induced (Figure 5A-B). Upon direct co-culture, we observed a massive induction  
297 of TNF- $\alpha$ , IFN- $\gamma$ , granzyme B, IL-10 and IL-17, irrespective of the activation state of CD8<sup>+</sup>  
298 T cells (Figure 5C-D). Altogether, these results show that soluble factors and direct contacts  
299 between fibrocytes and CD8<sup>+</sup> T cells might have an additive effect on CD8<sup>+</sup> T cell cytokine  
300 production. The concentration of TNF- $\alpha$  measured in culture supernatant increased  
301 significantly upon co-culture between fibrocytes and non-activated CD8<sup>+</sup> T cells at day 4,  
302 confirming that TNF- $\alpha$  was secreted in the medium upon direct interactions with fibrocytes  
303 (Figure 5E). This shows that both soluble factors produced by fibrocytes and direct contacts  
304 influence CD8<sup>+</sup> T cell secretion profile.

305 We then wondered whether glucocorticoid drugs (*i.e.*, budesonide or fluticasone propionate)  
306 could reverse the fibrocyte-induced proliferation and differentiation of CD8<sup>+</sup> T cells.  
307 Treatment with glucocorticoid drugs significantly decreased fibrocyte-induced TNF- $\alpha$   
308 secretion by non-activated CD8<sup>+</sup> T cells, without affecting the proliferation (Figure S10).  
309 Collectively, these results underline the importance of the interaction with fibrocytes for

310 CD8<sup>+</sup> T cell activation, possibly by favoring cellular proliferation and local cytokine  
311 production.

312

313

314 **Stochastic mathematical model taking into account intercellular interactions describes**  
315 **the evolution over time of cell populations in control and COPD bronchi**

316 All the above mentioned results led us to hypothesize that fibrocyte infiltration into the lung,  
317 differential migration of fibrocytes towards CD8<sup>+</sup> T cells and subsequent CD8<sup>+</sup> T cell  
318 proliferation, could result in a distinct spatial cellular repartition observed in tissues  
319 obtained from patients with COPD, compared to control tissues. To investigate this  
320 hypothesis, which could not be experimentally tested, we developed an agent-based  
321 (cellular automata) model with local and random cellular interactions. We considered the  
322 lamina propria (*i.e.*, the peribronchial zone), located between the bronchial epithelium and  
323 the smooth muscle layer, which contains fibrocytes and CD8<sup>+</sup> T cells. In line with the  
324 present analysis, the computational domain (*i.e.*, the lamina propria), corresponds to a zone  
325 of 179 000  $\mu\text{m}^2$ . Fibrocytes and CD8<sup>+</sup> T cell are considered as individual objects that can  
326 move, divide, die and infiltrate the lamina propria at the stable state and during exacerbation.  
327 Their individual behaviors and interactions are supposed to be stochastic and the value of  
328 the probabilities has been established from literature (Afroj et al., 2021; Bivas-Benita et al.,  
329 2013; Dupin et al., 2016, 2019; Ely et al., 2006; Freeman et al., 2007; Gribben et al., 1995;  
330 Hurst et al., 2010; Ling et al., 2019; McMaster et al., 2015; Mrass et al., 2017; Saetta et al.,  
331 1999; Scheipers & Reiser, 1998; Schmidt et al., 2003; Schyns et al., 2019; Siena et al., 2011;  
332 Takamura et al., 2016; Zenke et al., 2020) and the present *in vitro* data, as summarized in  
333 the method section and in Tables S9 and S10, and exhaustively described in the  
334 supplementary text and (Dupin et al., 2022). Initial cell densities were scaled with respect

335 to reference values, corresponding to the mean densities measured in non-smoking subjects.  
336 Simulations started with these initial densities and ended 20 years later, to reflect the average  
337 time between the beginning of cigarette smoke exposure and COPD onset (Løkke et al.,  
338 2006).

339 All the biological processes are governed by probabilities (Figure 6A). CD8<sup>+</sup> T cells, but  
340 not fibrocytes, are able to proliferate, based on our own unpublished observations and other  
341 studies (Ling et al., 2019; Schmidt et al., 2003). The presence of fibrocytes in the local  
342 neighborhood of a CD8<sup>+</sup> T cell can trigger CD8<sup>+</sup> T cell division with increased probability,  
343 based on the present *in vitro* experiments showing that the contact between those two cell  
344 types greatly enhanced CD8<sup>+</sup> T cell proliferation. Fibrocytes and CD8<sup>+</sup> T cells movements  
345 depend on the local neighborhood of cells, reflecting their relative chemo-attractive  
346 properties. We then simulated the evolution over 20 years, with two sets of parameters,  
347 respectively for the control and COPD cases and the second for the COPD case (see  
348 supplementary text).

349 We first tested the results of simulations against our experimental data from patients'  
350 tissues. First, we compared cell densities, experimentally measured in tissue samples, with  
351 theoretical predictions at the final state. Snapshots of the peribronchial area at the end of the  
352 simulations show that the densities of cells as well as their relative distribution were  
353 different between healthy and COPD situations (Figure 6B). From the simulations (n=160  
354 in each condition), we found a median of 754 CD8<sup>+</sup> T cells/mm<sup>2</sup> (95% CI, 748 to 763) and  
355 106 fibrocytes/mm<sup>2</sup> (95% CI, 101 to 108) in the control situation, and 1187 CD8<sup>+</sup> T  
356 cells/mm<sup>2</sup> (95% CI, 1169 to 1195) and 212 fibrocytes/mm<sup>2</sup> (95% CI, 206 to 216) in the  
357 COPD situation. These values are in very good agreement with our experimental findings,  
358 and the simulations were also able to reproduce the statistical increase of cell densities in  
359 COPD situation compared to that of controls (Figure 6C). Next, we tested if our theory

360 accounted for the experimental relative distribution of CD8<sup>+</sup> T cells and fibrocytes. The  
361 densities of CD8<sup>+</sup> T cells in interaction with fibrocytes (Figure 6D), the mean minimal  
362 distances between fibrocytes and CD8<sup>+</sup> cells (Figure 6E), the distribution of mean minimal  
363 distances (Figure S11) and the mean number of mixed cell clusters (Figure 6F) were in good  
364 agreement with tissular analyses and mimicked the variations observed between control  
365 subjects and patients with COPD. The densities of mixed cell clusters predicted by  
366 simulations (control simulations: median = 17 clusters/mm<sup>2</sup> (95% CI, 18 to 21), COPD  
367 simulations: median = 45 clusters/mm<sup>2</sup> (95% CI, 46 to 51), P<0.001) agreed perfectly with  
368 experimental measurements (Figure 6G) and were therefore chosen as a readout of  
369 intercellular interactions in the following analyses. If purely random, the density of mixed  
370 clusters was expected to be 28 clusters/μm<sup>2</sup> (95% CI, 25 to 29) and 73 clusters/μm<sup>2</sup> (95%  
371 CI, 70 to 74) in control and COPD situations, respectively (Figure S12). These random  
372 densities as well as the others parameters quantifying the relative distribution of cells were  
373 statistically different from the distributions obtained in both simulations and *in situ* analyses  
374 (Figure S12). We conclude that the relative organization of CD8<sup>+</sup> T cells and fibrocytes in  
375 control and COPD bronchi did not result from a pure stochastic mechanism but implicates  
376 chemotaxis processes.

377 One of the strengths of the model is to allow the monitoring of the temporal evolution of  
378 the different cellular processes and the numerical detection of a change of regime (Figure  
379 6H-I). CD8<sup>+</sup> T cells infiltration remained identical in control and COPD situation.  
380 Fibrocyte-induced T cell proliferation, that represents the minor part of the total  
381 proliferation in control situation, quickly increased in COPD situation over time to reach a  
382 plateau after approximately 4 years. As the basal proliferation of CD8<sup>+</sup> T cells remained  
383 similar in healthy and diseased situations, the resulting total proliferation in CD8<sup>+</sup> T cells  
384 over time was higher in the COPD situation compared to the control one. COPD dynamics



385 also affected CD8<sup>+</sup> T cell death, with a concomitant increase of T cell-induced death. In  
386 total, the net balance between gain and loss of CD8<sup>+</sup> T cells was around zero for control  
387 dynamics and strictly positive for COPD dynamics, explaining the increased CD8<sup>+</sup> T cell  
388 density in COPD simulations. Fibrocytes infiltration remained very similar in control and  
389 COPD dynamics (Figure 6I). Fibrocytes death was initially lower in COPD simulations  
390 before increasing and reaching a stationary state after approximately 7 years, resulting in a  
391 net expansion of fibrocytes population in COPD bronchi after 20 years. Moreover, the  
392 simulations allowed us to monitor the interactions between fibrocytes and CD8<sup>+</sup> T cells.  
393 The density of mixed cell clusters gradually increased in the first years of the COPD  
394 simulation before reaching a stationary state after approximately 6 years (Figure 6J, Movies  
395 S2 to S5). Altogether, the theory of the influence of local interactions tested by our agent-  
396 based (cellular automata) model correctly accounts for the shift of absolute and relative  
397 distribution of CD8<sup>+</sup> T cells and fibrocytes in peribronchial areas from control subjects to  
398 patients with COPD.

399

400

## 401 **Discussion**

402 The present study aimed at identifying the role and mechanism of fibrocyte-CD8<sup>+</sup> T cells  
403 cross-talk in COPD. A previous study had pointed out a pivotal role for fibrocyte to activate  
404 CD8<sup>+</sup> T cells proliferation (Afroj et al., 2021). However, whether and how both cell types  
405 could interact in bronchi, as well as their implication in COPD was completely unknown.  
406 Quantitative image analysis provided crucial insight into the relative distribution of  
407 fibrocytes and CD8<sup>+</sup> T cells in distal bronchial specimens from control subjects and COPD  
408 patients. In addition to data from previous studies demonstrating that the densities of both  
409 fibrocytes (Dupin et al., 2019) and CD8<sup>+</sup> T cells (Saetta et al., 1999) are increased within

410 the distal bronchi of COPD patients, we found that fibrocyte and CD8<sup>+</sup> T cells are localized  
411 in close proximity in peribronchial areas, especially in tissues from patients with COPD.  
412 We deciphered the spatiotemporal characteristics of these cell–cell contacts by live imaging  
413 in an *in vitro* autologous co-culture assay, and showed that the duration of the contacts was  
414 compatible with activation through the establishment of dynamic synapses. On the one  
415 hand, CD8<sup>+</sup> T cells induced fibrocyte chemotaxis, and, on the other hand, fibrocytes directly  
416 induced CD8<sup>+</sup> T cell proliferation and cytokine production. The strength of our work relies  
417 on the integration of findings from the present *in vitro* experiments and other studies into a  
418 comprehensive computational model that provides an accurate prediction of histological *ex*  
419 *vivo* characteristics opening up the possibility to figure out the *in vivo* effect of drugs in  
420 future studies. Altogether, our data suggest a pivotal role for fibrocytes to activate CD8<sup>+</sup> T  
421 cell deleterious functions in the context of COPD.

422  
423 We analyzed the relationship between these histological parameters and clinical data and  
424 found associations between fibrocyte presence, fibrocyte-CD8<sup>+</sup> T cell interaction and the  
425 alteration of lung function. We have demonstrated using stepwise and multivariate  
426 regressions that the density of interacting cells and the density of mixed cell cluster were  
427 the two best correlated parameters with the FEV<sub>1</sub>/FVC ratio, supporting a potential role for  
428 the interplay between both cell types in COPD. Since regions of microscopic  
429 emphysematous destruction of terminal bronchioles have been associated with increased  
430 infiltration of CD8<sup>+</sup> T cells and immune response activation, such as the up-regulation of  
431 IFN- $\gamma$  signaling (Xu et al., 2021), it is tempting to speculate that fibrocyte-CD8<sup>+</sup> T cell  
432 interplay could be implicated in early changes leading to tissue remodeling and chronic  
433 inflammation in COPD. Of note, the gene signature obtained by tissue microarray associated  
434 with this site also indicates the modification of two genes associated with the tissue repair

435 process, FGF10 and TGFB2 (Xu et al., 2021). Considering the possible effect of CD8<sup>+</sup> T  
436 cells on fibrocyte differentiation, it could be worthwhile to focus on these genes in further  
437 studies.

438  
439 We also addressed the potential mechanisms explaining these increased interactions of  
440 CD8<sup>+</sup> T cells and fibrocytes in tissues of COPD patients. Chemotaxis could guide CD8<sup>+</sup> T  
441 cells towards fibrocytes and reciprocally, as it has been proposed for T cells towards  
442 dendritic cells (Mackay, 2001; Ngo et al., 1998; von Andrian & Mackay, 2000). Stronger  
443 or longer interactions could also explain the differential spatial distribution between healthy  
444 and diseased tissues. On the other hand, the contact between both cell types could also occur  
445 through a stochastic mechanism, as shown for CD4<sup>+</sup> T cells and dendritic cells in lymph  
446 nodes, without any implication of chemotactic processes (Miller et al., 2004). Although we  
447 cannot totally rule out a role for fibrocyte-CD8<sup>+</sup> T cell adhesion to explain the increased  
448 interactions, our findings rather suggest a central role for the CXCL8-CXCR1/2 axis in  
449 promoting encounters between CD8<sup>+</sup> T cells and fibrocytes in COPD patients. Importantly,  
450 this is further supported by the results of computational modelization, which only integrates  
451 chemotaxis and not adhesion processes, revealing a final spatial repartition of cells in the  
452 COPD situation distinct from a random distribution. Altogether, our data suggest that the  
453 likelihood of interactions between fibrocytes and CD8<sup>+</sup> T cells could be increased in tissues  
454 from patients with COPD through the CXCL8-CXCR1/2 axis thus participating to cluster  
455 fibrocytes and CD8<sup>+</sup> T cells in diseased tissues. Importantly, dual blockers of CXCR1-  
456 CXCR2 have been suggested as therapeutic targets in COPD (Henrot et al., 2019) and are  
457 efficient in our *in vitro* experiments to block the increased chemotaxis of fibrocytes towards  
458 secretion of CD8<sup>+</sup> T cells purified from COPD tissues. The outcome of such therapies could  
459 be predicted using the computational model described in this study.

460

461

462

463

464

465

466

467

468

469

470

471

472

473

474

475

476

477

478

479

480

481

482

483

484

We show that fibrocytes act as a major promoter on CD8<sup>+</sup> T cell proliferation, thus confirming, in an autologous co-culture system, what has been previously found in the context of cancer-related immunity (Afroj et al., 2021). This is consistent with the present *in situ* analyses, showing the presence of clusters containing both cell types in peribronchial area, especially in the tissues from patients with COPD. The mean numbers of cells in those clusters remained relatively low, suggesting that these structures are distinct from inducible bronchus-associated lymphoid tissue (iBALT) (Conlon et al., 2020). Although a previous report has demonstrated that fibrocytes, exposed to viral antigens, could induce proliferation of naïve CD8<sup>+</sup> T cells (Balmelli et al., 2005), the pro-proliferative effect exerted by fibrocytes on CD8<sup>+</sup> T cells occurred without antigen exposure in our *in vitro* study. This antigen-independent T cell proliferation driven by fibrocytes was also found in the context of sepsis (Nemzek et al., 2013), suggesting that fibrocytes generally impact T cells expansion with a mechanism independent of the traditional antigen-driven clonal proliferation. This is also in agreement with our findings showing that contacts between CD8<sup>+</sup> T cells and fibrocytes were relatively short and dynamic, and that the dynamics of the interaction did not depend on the activation state of CD8<sup>+</sup> T cells. The spatiotemporal behavior of CD8<sup>+</sup> T cells was consistent with the establishment of dynamic synapse, also called “kinapse” (Dustin, 2008), which are associated with the induction of relatively weak TCR signals (Moreau et al., 2012). We have evidenced the requirement for cellular contacts, implicating the surface receptors CD86 and CD54. The lack of effect of the anti-CD86 and CD54 in pre-activated CD8<sup>+</sup> T cells might indicate potential changes of expression of molecules belonging to the immunological synapse upon activation, that could make the lymphocytes more responsive to others signals. The well-known inhaled corticosteroids (*i.e.*, budesonide and fluticasone propionate) also failed to significantly inhibit fibrocyte-

485 induced CD8<sup>+</sup> T cell proliferation. This is consistent with their lack of activity in  
486 lymphocytes obtained from patients with COPD (Kaur et al., 2012). In contrast, we propose  
487 that targeting the interaction between structural and immune cells and/or its consequences  
488 should reveal robust candidates for future pharmacotherapeutic strategies to treat COPD. Of  
489 note, the stimulatory activity of CD8<sup>+</sup> T cells by fibrocytes was also found to be enhanced  
490 by the blockade of the PD-1/PD-L1 pathway in a previous study (Afroj et al., 2021). As this  
491 latter property of fibrocytes may be beneficial in tumor microenvironment (Henrot et al.,  
492 2021), especially when cancer patients were treated with anti-PD-1/PD-L1 antibody, it  
493 might be rather detrimental in COPD patients, by promoting tissue damages and chronic  
494 immune inflammation.

495  
496 Fibrocytes skewed CD8<sup>+</sup> T-cell populations towards both CD8<sup>high</sup> and CD8<sup>low</sup> phenotypes  
497 in a cell–cell contact independent manner. It has been described that, following contact  
498 between an antigen presenting cell and a lymphocyte, asymmetric division can occur  
499 generating a memory cell, weakly expressing CD8, and an effector cell strongly expressing  
500 CD8 (Backer et al., 2018; J. T. Chang et al., 2007). The asymmetry is reduced but still  
501 present even without specific recognition of foreign antigen by T cells (J. T. Chang et al.,  
502 2007). It is tempting to speculate that the induced proliferation we observed in our  
503 experiments generates, via asymmetric division, unequal CD8 inheritance in daughter cells.  
504 The low level of cytokine expression in CD8<sup>low</sup> cells is compatible with an exhausted  
505 phenotype, while CD8<sup>high</sup> cells express higher levels of cytokines, a profile consistent with  
506 an effector commitment. Although the presence of the CD8<sup>high</sup> and CD8<sup>low</sup> subsets remain  
507 to be evidenced in the tissues, we suspect that the relative expansion of the CD8<sup>high</sup> and  
508 CD8<sup>low</sup> subset triggered by fibrocytes could have functional implications. Reiterative rounds  
509 of CD8<sup>+</sup> T cells division induced by frequent interactions with fibrocytes might induce

510 defective immune response by exhausted CD8<sup>low</sup> T cells (Grundy et al., 2013; McKendry et  
511 al., 2016), and tissue destruction by cytotoxic CD8<sup>high</sup> cells (Chrysofakis et al., 2004; Maeno  
512 et al., 2007).

513  
514 In COPD, outside of exacerbations, factors triggering pro-inflammatory cytokines  
515 production are still elusive. Here, we demonstrate that fibrocytes exert a strong effect  
516 through soluble factors and direct cellular contacts with CD8<sup>+</sup> T cells, inducing a massive  
517 upregulation of TNF- $\alpha$ , IFN- $\gamma$  and granzyme B production, all implicated in COPD  
518 pathophysiology (Barnes, 2016). Greater production of TNF- $\alpha$ , IFN- $\gamma$  and granzyme B by  
519 CD8<sup>+</sup> T cells triggered by the interaction with fibrocytes is consistent with previous studies  
520 showing enhanced production of Tc1 cytokines and cytotoxic molecules by CD8<sup>+</sup> T cells  
521 purified from patients with COPD (Freeman et al., 2010; Hodge et al., 2007; Lethbridge et  
522 al., 2010), suggesting that local interactions with cells such as fibrocytes may play a pivotal  
523 role in CD8 polarization in COPD. In particular, TNF- $\alpha$  has proinflammatory and  
524 prooxidative actions (Mukhopadhyay et al., 2006), and its overexpression has been  
525 associated with emphysema (Lundblad et al., 2005). TNF- $\alpha$  can directly contribute to  
526 cytolysis, together with the cytotoxic granzyme B (Velotti et al., 2020) and in synergy with  
527 IFN- $\gamma$  (Williamson et al., 1983). TNF- $\alpha$  can also indirectly participate to extracellular matrix  
528 degradation through the induction of matrix metalloproteinases (Wright et al., 2007).  
529 Simultaneously, the production of the pro-fibrotic IL-17 was also induced upon co-culture  
530 with fibrocytes, raising the possibility that the interaction between CD8<sup>+</sup> T cells and  
531 fibrocyte participates to the generation of IL-17-secreting CD8<sup>+</sup> T cells in airways of  
532 patients with COPD (Y. Chang et al., 2011). Interestingly, IL-17 is able to simulate matrix  
533 components synthesis in other cell types, including fibrocytes, and promotes CD40-  
534 mediated IL-6 production by fibrocytes (Hayashi et al., 2013). Cooperative interactions

535 between fibrocytes and CD8<sup>+</sup> T cells, through tissue destruction and abnormal matrix  
536 components synthesis, may thus directly contribute to the loss of normal lung function. On  
537 the other hand, CD8<sup>+</sup> T cell production of anti-inflammatory cytokines such as IL-10, was  
538 also stimulated upon co-culture with fibrocytes. In total, rather than the net production of  
539 each cytokine, it is probably the balance or imbalance between pro-inflammatory and anti-  
540 inflammatory molecules that will dictate the outcome of the inflammatory process.

541  
542 Whereas the field of respiratory research is rapidly moving towards an exhaustive  
543 description of modifications of molecular and cellular components in diseased lungs, the  
544 actual transition between a healthy to a diseased state, although critical, remains very  
545 difficult to investigate. We developed here a probabilistic cellular automata type model to  
546 explore of dynamic behaviors and interactions between fibrocytes and CD8<sup>+</sup> T cells.  
547 Previous agent-based computational approaches have been used to describe the switch from  
548 normal to allergic response (Pothen et al., 2015) and airway remodeling in asthma (Saunders  
549 et al., 2019), but, to our knowledge, this type of modeling was never applied to COPD.  
550 Qualitative estimates of probabilities that govern cell death, proliferation, infiltration and  
551 displacement are derived from experimental data from our study and others. We could  
552 simulate spatiotemporal behaviors of cells in the lamina propria over long period of time  
553 (*i.e.*, 20 years) and we showed that this model can accurately reproduce the absolute and  
554 relative repartition of fibrocytes and CD8<sup>+</sup> T cells in both control and COPD situations.

555 Although simulated and *in situ* data were close, the variances of *in silico* data were smaller  
556 than the *in situ* measurements, which can be probably explained by the fact that cell diversity  
557 and interactions are far more complex than those considered in this model. Nevertheless, it  
558 appears that (i) our model captures important aspect of reality, and (ii) modifications of  
559 specific cellular processes and local interactions, *i.e.* fibrocyte-induced CD8<sup>+</sup> T cell

560 proliferation and fibrocyte attraction towards CD8<sup>+</sup> T cells, are sufficient to reproduce the  
561 shift of histological composition between the control and COPD situations. This theoretical  
562 approach and associated simulations allowed us to validate the key hypothesis of  
563 modification of local interactions, and to show that the specific values of the COPD  
564 parameters led to an increased cell density and the spatial patterns observed in patients with  
565 COPD. The simulations made it possible to follow over time various quantities of interest  
566 and to empirically determine the time when the stationary state is achieved, that would be  
567 difficult to reveal in any other way. Given the consistency of our results with those from the  
568 literature, our model provides a unique opportunity to decipher the dynamics of increased  
569 interactions between the two cell types as well as the infinite possibility to investigate  
570 therapeutic strategies.

571  
572 The present *in vitro* model has limitations, including the use of circulating cells for some *in*  
573 *vitro* experiments and the difficulty in extrapolating results obtained from these assays to *in*  
574 *vivo* processes. However, we took this limit into account in our modelization approach, by  
575 using a combination of our experiments and measurements obtained in tissues, to accurately  
576 determine the dedicated parameters (Dupin et al., 2022). Even if computational  
577 modelization was done in 2D, whereas the bronchi are 3D structures, we believe that our  
578 model is representative as it mimics the cellular distribution of normal and pathological  
579 airways, that was also quantified in 2D lung sections. Besides this, some quantitative  
580 features of our approach are still valid in 3D, such as the probabilities that govern cell death,  
581 proliferation and infiltration, whereas others are expected to change with dimensionality,  
582 such as displacement rules.



584 From our study and others (Hufford et al., 2011; Takamura et al., 2019), it is now clear that  
585 the fate of CD8<sup>+</sup> T cells in distal airways may depend on multiple successive interactions  
586 with different cell types, including fibrocytes. We believe that targeting interaction between  
587 structural and immune cells should be considered in future drug discovery programs and  
588 that computational modelization should help to refine drug priority.

## 589 **Materials and Methods**

### 590 **Study Populations**

591 Lung tissues for the *in situ* study were obtained from a previously described cohort (Dupin  
592 et al., 2019). Briefly, subjects more than 40 years of age were eligible for enrolment if they  
593 required thoracic lobectomy surgery for cancer (pN0), lung transplantation or lung volume  
594 reduction. A total of 17 COPD patients with a clinical diagnosis of COPD according to the  
595 GOLD guidelines (Global Initiative for Chronic Obstructive Lung Disease, 2022) and 25  
596 non-COPD subjects (“control subjects”) with normal lung function testing (*i.e.*, FEV<sub>1</sub>/FVC  
597 > 0.70) and no chronic symptoms (cough or expectoration) were recruited from the  
598 University Hospital of Bordeaux.

599 Lung tissues for the purification of tissular CD8<sup>+</sup> T cells were obtained from a separate  
600 cohort of patients. A total of 17 patients with COPD and 23 nonsmokers were prospectively  
601 recruited from the University Hospital of Bordeaux, according to the GOLD guidelines  
602 (Global Initiative for Chronic Obstructive Lung Disease, 2022) (Table S7). Fragments of  
603 distal parenchyma from all subjects were obtained by either lobectomy or transplantation.  
604 To study fibrocyte- CD8<sup>+</sup> T cells interplay *in vitro*, blood samples were obtained from a  
605 separate cohort of COPD patients, (*i.e.*, COBRA (Bronchial Obstruction and Asthma  
606 Cohort; sponsored by the French National Institute of Health and Medical Research,  
607 INSERM), as outpatients in the Clinical Investigation Centre of the University Hospital of  
608 Bordeaux (Table S8).

609 All subjects gave their written informed consent to participate to the studies. The studies  
610 received approval from the local or national ethics committees.

611

### 612 **Identification of bronchial fibrocytes and CD8<sup>+</sup> T cells**

613 Fragments of distal parenchyma were obtained from macroscopically normal lung resection  
614 or transplantation material. The samples were embedded in paraffin and sections of 2.5  $\mu\text{m}$   
615 thick were cut, as described previously (Dupin et al., 2019). Sections were deparaffinized  
616 through three changes of xylene and through graded alcohols to water. Heat induced antigen  
617 retrieval was performed using citrate buffer, pH 6 (Fisher Scientific, Illkirch, France) at  
618 96°C in a Pre-Treatment Module (Agilent, Les Ulis, France). Endogenous peroxidases were  
619 blocked for 10 min using hydrogen peroxide treatment (Agilent). Nonspecific binding was  
620 minimized by incubating the sections with 4% Goat Serum (Agilent) for 30 min, before  
621 CD8 staining, and before the double staining for CD45 and FSP1. First, the sections were  
622 stained with rabbit anti-CD8 monoclonal antibody (Fisher Scientific) during 45 min, and  
623 then incubated with HRP anti-Mouse (Agilent). Immunoreactivity was detected by using  
624 the DAB System (Agilent). Second, the same sections were stained with mouse anti-CD45  
625 monoclonal antibody (BD Biosciences, San Jose, CA) overnight and then with rabbit anti-  
626 FSP1 polyclonal antibody (Agilent) during 45 min. They were incubated with Alexa568-  
627 conjugated anti-Mouse and with Alexa488-conjugated anti-Rabbit (Fisher Scientific)  
628 antibodies. Immunoreactivity was detected by fluorescence for FSP1 and CD45 staining.  
629 The sections were imaged using a slide scanner Nanozoomer 2.0HT with fluorescence  
630 imaging module (Hamamatsu Photonics, Massy, France) using objective UPS APO 20X  
631 NA 0.75 combined to an additional lens 1.75X, leading to a final magnification of 35X.  
632 Virtual slides were acquired with a TDI-3CCD camera. Fluorescent acquisitions were done  
633 with a mercury lamp (LX2000 200W - Hamamatsu Photonics) and the set of filters adapted  
634 for DAPI, Alexa 488 and Alexa 568. Bright field and fluorescence images were acquired  
635 with the NDP-scan software (Hamamatsu) and processed with ImageJ.  
636 Quantification of CD8<sup>+</sup> T cells was performed, as described in Figure S1A, C. A color  
637 deconvolution plugin was used on brightfield image to isolate the signal corresponding to

638 DAB staining. A binary threshold was applied to this grayscale image, followed by a  
639 watershed transformation to the segmented image to separate potential neighboring cells  
640 (Figure S1C). CD8<sup>+</sup> T cells were then automatically counted by recording all the positive  
641 particles with an area greater than 64  $\mu\text{m}^2$ . This threshold was empirically determined on  
642 our images to select positive cells. Quantification of dual positive cells for FSP1 and CD45  
643 was performed, as described in Figure 1B, D. A binary threshold was applied to fluorescence  
644 images corresponding to FSP1 and CD45 stainings. These images were combined using the  
645 “AND” function of the Fiji “Image Calculator” to select cells dual positive for FSP1 and  
646 CD45 double staining (Figure S1D). This was followed by a watershed transformation to  
647 separate potential neighboring cells. These CD45<sup>+</sup> FSP1<sup>+</sup> cells were then automatically  
648 counted by recording all the positive particles with an area greater than 64  $\mu\text{m}^2$ .

649  
650 **Quantification of the density of CD8<sup>+</sup> T cells, FSP1<sup>+</sup> CD45<sup>+</sup> cells and CD8<sup>+</sup> T cells in**  
651 **interaction with CD45<sup>+</sup> FSP1<sup>+</sup> cells**

652 This latter segmented image was then used to quantify CD8<sup>+</sup> T cells in interaction with  
653 CD45<sup>+</sup> FSP1<sup>+</sup> cells as described in Figure 1E: each CD8 positive particle with an area  
654 greater than 64  $\mu\text{m}^2$  was enlarged using the dilatation function (4, 8, 10 and 15 pixels  
655 dilatation: used to count the cells respectively less than 1.8, 3.6, 4.5 and 6.8  $\mu\text{m}$  apart). This  
656 modified image was combined with the segmented image for dual CD45 FSP1 positive  
657 staining using the “AND” function of the Fiji “Image Calculator” to select CD8<sup>+</sup> T cells in  
658 interaction with CD45<sup>+</sup> FSP1<sup>+</sup> cells. These interacting cells were automatically counted by  
659 recording all the positive particles. The lamina propria contour was manually determined  
660 on bright field image and the area was calculated. For distal bronchi, the lumen area was  
661 also determined and only bronchi less than 2 mm in diameter were analyzed as described  
662 previously (Hogg et al., 2004). The densities of CD8<sup>+</sup> T cells, FSP1<sup>+</sup> CD45<sup>+</sup> cells and

663 interacting cells were defined by the ratio between the number of positive cells in the lamina  
664 propria divided by lamina propria area. Tissue area and cell measurements were all  
665 performed in a blinded fashion for patients' characteristics.

### 666 **Quantification of the minimal distances between CD45<sup>+</sup> FSP1<sup>+</sup> cells and CD8<sup>+</sup> T cells**

667 The segmented image produced from the DAB staining image was inverted, and a CD8  
668 distance map was built from the latter image (Figure S1F). As a result, the brighter the pixel,  
669 the closer the distance from a CD8<sup>+</sup> T cell. Conversely, the darker the pixel, the farther away  
670 the distance from a CD8<sup>+</sup> T cell. On the binary image produced from FSP1 and CD45  
671 staining images, dual positive cells for FSP1 and CD45 were selected in the lamina propria.  
672 Each area corresponding to a FSP1<sup>+</sup> CD45<sup>+</sup> cell was reported on the CD8 distance map, and  
673 the minimal gray value in each area was measured and converted to a distance, allowing to  
674 measure the minimal distance between the CD45<sup>+</sup> FSP1<sup>+</sup> cell and neighboring CD8<sup>+</sup> T cells.  
675 For each patient, a frequency distribution of all minimal distances (with 7  $\mu$ m binning) and  
676 the mean minimal distance were calculated.  
677

### 678 **Quantification of cell clusters**

679 On the segmented image with dual CD45 FSP1 positive staining combined with CD8  
680 positive staining, centroids from positive particles located in the lamina propria were  
681 connected by a Delaunay triangulation, using a custom freely available ImageJ plugin  
682 (Schneider et al., 2012) (Figure S3A-C, [https://github.com/fle vet/Delaunay\\_clustering\\_ImageJ](https://github.com/fle vet/Delaunay_clustering_ImageJ)). All triangles sharing one edge with  
683 the ROI defining the lamina propria were removed (Figure S3C, left panel). On the  
684 remaining triangulation a distance threshold, corresponding to the minimal mean distance  
685 between fibrocytes and CD8<sup>+</sup> T cells (40  $\mu$ m) was applied, allowing to select the  
686  
687

688 connections with a distance lower than the threshold distance (Figure S3C, right panel). The  
689 number of clusters and their composition were then automatically recorded.

690

### 691 **Fibrocyte and CD8<sup>+</sup> T cell purification**

692 Peripheral blood mononuclear cells (PBMCs) were first separated from the whole blood by  
693 Ficoll-Hypaque (Eurobio Scientific, Les Ulis, France) density gradient centrifugation. Cells  
694 were washed twice in cold PBS containing 0.5% bovine serum albumin (BSA, Sigma-  
695 Aldrich, Saint Quentin-Fallavier, France) and 2 mM Ethylene Diamine Tetra-acetic Acid  
696 (EDTA, Invitrogen, Cergy Pontoise, France). CD8<sup>+</sup> T cells were purified by positive  
697 selecting using CD8 microbeads (Miltenyi Biotech, Paris, France). CD8<sup>+</sup> T cells were  
698 washed in a buffered solution (“CTL-Wash™”, Cellular Technology Limited, Bonn,  
699 Germany) and resuspended in a serum-free freezing media (“CTL-Cryo™ Medium”,  
700 Cellular Technology Limited, Bonn, Germany) for cryopreservation of freshly-isolated  
701 CD8<sup>+</sup> T cells during fibrocyte differentiation. The CD8<sup>+</sup> T cells-depleted cell fraction was  
702 then depleted from CD3<sup>+</sup> cells using CD3 microbeads (Miltenyi Biotec). Cell suspension  
703 containing fibrocyte precursors was cultured during at least 14 days to induce fibrocyte  
704 differentiation: a total of  $2 \cdot 10^6$  cells resuspended in 1 ml DMEM (Fisher Scientific, Illkirch,  
705 France), containing 4.5 g/l glucose and glutaMAX, supplemented with 20% fetal calf serum  
706 (Biowest, Riverside, USA), penicillin/streptomycin and MEM non-essential amino acid  
707 solution (Sigma-Aldrich), was added to each well of a 12 well plate. After one week in  
708 culture, fibrocyte differentiation was induced by changing the medium for a serum-free  
709 medium. Mediums were changed every 2-3 days.

710

### 711 **Fibrocyte/CD8<sup>+</sup> T cells co-culture assay**

712 One day before co-culture, CD8<sup>+</sup> T cells were thawed. A buffer solution previously heated  
713 to 37°C (PBS 1X with 0.5% BSA and 2mM EDTA) was added to the cell suspension. CD8<sup>+</sup>  
714 T cells were washed with PBS and resuspended in DMEM supplemented with 8% fetal calf  
715 serum for a final concentration of 0.5.10<sup>6</sup> cells/mL. CD8<sup>+</sup> T cells were either stimulated  
716 with a low dose of CD3 antibody (3μg / 10<sup>6</sup> cells) to promote cell survival without  
717 stimulating cell proliferation (“non-activated” condition), or stimulated overnight with anti-  
718 CD3/CD28 coated microbeads (Fisher Scientific) with a bead-to-cell ratio of 1:1  
719 (“activated” condition). At day 0 (co-culture), these beads were removed, CD8<sup>+</sup> T cells were  
720 stained with 5 μM CellTrace Violet (Fisher Scientific) in case of proliferation experiments,  
721 before being added to fibrocyte cultures (0.5.10<sup>6</sup> CD8<sup>+</sup> T cells/well). In blocking  
722 experiments, the antibodies (Abs) directed against LFA-1 (clone HI111, BioLegend,  
723 1μg/mL), CD54 (clone HA58, eBioscience), CD86 (clone IT2.2, eBioscience, 10μg/mL) or  
724 CD44 (clone 82102, Biotechne, 10μg/mL) were used with their respective control Abs,  
725 mIgG1 κ (clone MOPC-21, BioLegend), mIgG2b κ (eBM 2b, eBioscience), mIgG2B  
726 (133303, Biotechne). In LFA-1 and CD44 blocking experiments as well as in glucocorticoid  
727 drugs experiments, CD8<sup>+</sup> T cells were preincubated respectively with corresponding Abs,  
728 budesonide or fluticasone propionate (10<sup>-8</sup>M, MedChemExpress) at 37°C for 1h before  
729 being added to fibrocytes. In CD54 and CD86 blocking experiments, fibrocytes were  
730 preincubated with corresponding Abs at 37°C for 1h before adding CD8<sup>+</sup> T cells. For  
731 indirect co-culture, CD8<sup>+</sup> T cells were cultured in 0.4 μm transwell inserts (Sigma-Aldrich)  
732 for 12-well plates.

### 734 **Live imaging**

735 For time-lapse microscopy, cells were imaged after 2 days of co-culture, at 37°C and with  
736 5% CO<sub>2</sub> on an inverted DMi8 stand microscope (Leica, Microsystems, Wetzlar, Germany)

737 equipped with a Flash 4.0 sCMOS camera (Hamamatsu, Japan). The objective used was a  
738 HC PL FL L 20X dry 0.4 NA PH1. The multi-positions were done with a ASI MS-2000-  
739 500 motorized stage (Applied Scientific Instrumentation, Eugene, USA). The 37°C/5%CO<sub>2</sub>  
740 atmosphere was created with an incubator box and an gaz heating system (Pecon GmbH,  
741 Erbach, Germany). This system was controlled by MetaMorph software (Molecular  
742 Devices, Sunnyvale, USA). Phase contrast images were collected every 2 min for 12h.  
743 Image analysis and measurements were performed with the ImageJ software. Using the  
744 plugin "Cell counter " of the Fiji software, the number of CD8<sup>+</sup> T cells in direct contact with  
745 a fibrocyte as well as the number of free CD8<sup>+</sup> T cells were manually counted at the  
746 beginning of the acquisition and after 12 hours of acquisition. Cell tracking was performed  
747 using the "Manual Tracking" plugin of the Fiji software to determine the durations of  
748 contacts between tracked CD8<sup>+</sup> T cell with fibrocytes and the frequency of contact. A  
749 contact was defined manually by a direct interaction between CD8<sup>+</sup> T cell and fibrocyte.  
750 Five numerical variables were collected to characterize CD8<sup>+</sup> T cell dynamic over time. The  
751 mean speed corresponded to the track length divided by the time of tracking duration. The  
752 mean free speed corresponded the length of the track when the T cell was not interacting  
753 with any other cell, divided by the time spent free. The mean contact speed corresponded to  
754 the length of the track when the T cell is in contact with a fibrocyte, divided by the time  
755 spent in contact. For each T cell and for each contact, a contact time was defined as the time  
756 spent in contact until the T cell becomes free again. Then, each T cell can have many contact  
757 times with fibrocytes. The contact coefficient was defined by the proportion of time the T  
758 cell was in contact with a fibrocyte divided by the time of tracking duration.

759

760 **CD8<sup>+</sup> T cell characterization by flow cytometry**



761 Four or 6 days after co-culture, CD8<sup>+</sup> T cells were harvested and manually counted before  
762 being processed for FACS analysis. Intracellular cytokines were assessed following  
763 stimulation with PMA (25 ng/ml, Sigma-Aldrich), ionomycin (1 $\mu$ M, Sigma-Aldrich) for 4h  
764 and brefeldin A (5 $\mu$ g/ml, Sigma-Aldrich) for the last 3 h. Cells were stained with anti-CD8-  
765 PerCP-Vio700, anti-CD45-RA-FITC, and then fixed, permeabilized using the IntraPrep  
766 Permeabilization Reagent Kit (Beckman Coulter) and stained with anti-Granzyme-APC,  
767 anti-TNF- $\alpha$ -PE, anti-IFN- $\gamma$ -APC, anti-IL-17- PE-Cy7, anti-IL-10-PE or isotype controls  
768 (Miltenyi Biotech, Paris, France). The percentage of cell proliferation was estimated using  
769 Cell Trace Violet fluorescence loss. FACS data were acquired using a Canto II 4-Blue 2-  
770 Violet 2-Red laser configuration (BD Biosciences). Flow cytometry analysis were  
771 performed using Diva 8 (BD Biosciences). Human TNF- $\alpha$  concentration levels were  
772 quantified using ELISA following manufacturer's recommendations (BioTechne). Values  
773 below the detection limit were counted as zero.

#### 774

#### 775 **Dataset transcriptomic analysis**

776 The microarray data of tissular CD8<sup>+</sup> T cells was downloaded from the Gene Expression  
777 Omnibus (<http://www.ncbi.nlm.nih.gov/geo/>) using a dataset under the accession code  
778 GSE61397. Differential expression analysis between patients with COPD and control  
779 subjects was performed using the GEO2R interactive web tool. Heatmaps of the expression  
780 profiles for genes related to cell adhesion and chemotaxis were visualized with Graphpad  
781 Prism 6 software.

#### 782

#### 783 **Tissular CD8<sup>+</sup> T cell purification, culture and secretion profile analyses**

784 After lung parenchyma resection from control or COPD patients, samples were finely  
785 chopped at room temperature using scissors and then enzymatically dissociated with 40

786 IU/mL of collagenase (ThermoFisher) in DMEM medium for 45 min at 37°C. The  
787 enzymatic reaction was stopped by adding HBSS medium (Hank's Balanced Salt Solution)  
788 without calcium and supplemented with 2mM EDTA (Invitrogen, Cergy Pontoise, France).  
789 The cell suspension was filtered twice using 100 µm gauze and 70 µm cell strainer (Fisher  
790 Scientific). Tissue CD8<sup>+</sup> T cells were purified by positive selecting using CD8 microbeads  
791 (Miltenyi Biotech, Paris, France). Then, tissue CD8<sup>+</sup> T cells were resuspended in DMEM  
792 supplemented with 8% fetal calf serum, soluble anti-CD3 and anti-CD28 antibodies  
793 (respectively 1µg and 3µg for 10<sup>6</sup> cells) for a final concentration of 0.5 x 10<sup>6</sup> cells/mL. After  
794 36h, supernatants from tissue CD8<sup>+</sup> T cells were collected and frozen, for migration  
795 experiments or for further analyses. Supernatants from different samples obtained either  
796 from non-smoking subjects or patients from COPD were pooled for migration experiments.  
797 Supernatant concentration of CXCL8 was measured using ELISA (Biotechne). CCL26,  
798 CXCL2 and CCL2 concentrations were measured by using a customized Bio-Plex Assay  
799 (BioRad, Hercules, CA), using special plate reader (Bio-Plex 200 Systems, BioRad) and  
800 software (Bio-Plex manager), according to the manufacturer's instruction.

### 801 **Fibrocyte migration**

802 Fibrocytes precursors were isolated from peripheral blood as described previously (Dupin  
803 et al., 2016). Fibrocyte migration was assessed using a modified Boyden chamber assay.  
804 The transwell inserts (pore size 8 µm, Dutscher) and the wells were coated for 1h at room  
805 temperature with poly-lysine-ethylene glycol (PEG-PLL, SuSoS, Dübendorf, Switzerland)  
806 to prevent cell adhesion. A total of 0.3 x 10<sup>6</sup> NANT cells resuspended in 0.2 ml DMEM,  
807 containing 4.5 g/l glucose and L-glutamine, supplemented with penicillin/streptomycin and  
808 MEM non-essential amino acid solution were added to the upper compartment of each well.  
809 When indicated, NANT cells were pretreated for 30 min at 37°C with 200nM reparixin  
810

811 (MedChem Express), an antagonist of CXCR1-2. Supernatants of tissular CD8<sup>+</sup> T cells from  
812 non-smoking control subjects or COPD patients were added to the bottom compartment of  
813 each well. When indicated, supernatants were pretreated for 30 min at 37°C with blocking  
814 Ab against CXCL8 (clone 6217, BioTechne, 1µg/mL) or respective control Ab. After 12h,  
815 the content of bottom compartment was removed and DAPI staining was performed to  
816 exclude dying cells. Cells were then fixed, permeabilized and stained with anti-Collagen  
817 Type I-FITC (Sigma Aldrich), anti-CD45-APC (BD Pharmingen), anti-CXCR1-PE and  
818 anti-CXCR2-APC-Cy7 (Miltenyi Biotec, Paris, France). Fibrocyte migration was assessed  
819 by flow cytometry using double labeling CD45-Collagen I. To obtain absolute values of  
820 migratory cells, flow cytometric counts for each condition were obtained during a constant  
821 predetermined time period (1 min). The fraction of migratory fibrocytes was defined as the  
822 number CD45<sup>+</sup> Col1<sup>+</sup> cells counted in the bottom chamber divided by the number of total  
823 added cells. These values were normalized to the fraction of migratory fibrocytes obtained  
824 in the control condition.

## 825

### 826 **The mathematical model**

827 Exhaustive description of the mathematical model is provided in the supplementary text.  
828 To understand the interaction between fibrocyte and CD8<sup>+</sup> T cells in the spatial cellular  
829 organization in the peribronchial area, we constructed a discrete time cellular automata  
830 model. Two agent types are introduced - CD8<sup>+</sup> T cell agents and fibrocytes agents, denoted  
831 C and F respectively. C and F cells evolve on a lattice in two-dimensions. We take as surface  
832 of interest a zone with a crown shape, containing 3 652 lattice sites corresponding to a total  
833 area of approximately 179 000 µm<sup>2</sup>, which is in agreement with our *in situ* measurements.  
834 Reflecting (zero-flux) boundary conditions are imposed at the external and internal borders.  
835 On each site, there is at most one cell. The lattice is initially randomly seeded with both F

836 and C cells at densities corresponding at the mean distribution of non-smokers subjects,  
837 reflecting the “healthy” situation :  $n_0(C) = 660$  cells/mm<sup>2</sup>, and  $n_0(F) = 106$  cells/mm<sup>2</sup>. This  
838 corresponds to an average value of  $N_0(C) = 118$  C cells and  $N_0(F) = 19$  F cells.

839 We assumed that for a healthy subject as for a patient with COPD, the same model can be  
840 applied but with different parameters. These parameters are estimated thanks to experiments  
841 and data from the literature (see supplementary text and (Dupin et al., 2022) for a complete  
842 description, Table S10 for numerical values).

843 The notations and parameters of the mathematical model are summarized in Table S9 and  
844 their numerical values are given in Table S10. We now describe the behavior of the cells  
845 and their interactions. F and C cells infiltrate into the peribronchial area at the stable state  
846 with the respective probabilities  $p_{istaF}$  and  $p_{istaC}$ , and during exacerbation, a supplementary  
847 infiltration can occur, each year, with the probability  $p_{iexaF}$  (resp.  $p_{iexaC}$ ). In the model, C  
848 cells can proliferate with a very low probability  $p_C$ , but the presence of F cells in the local  
849 neighborhood of a C cell can induce C cell division with increased probability  $p_{C/F}$ , based  
850 on our own results and another study (Afroj et al., 2021). We suppose that fibrocytes do not  
851 proliferate, as shown by our own *in vitro* observations (data not shown) and other studies  
852 (Ling et al., 2019; Schmidt et al., 2003). F and C cells can move, with probabilities which  
853 are determined by the results from chemotaxis experiments (Figure 2). F and C cells die  
854 with a "basal" probability  $p_{dC}$  (respectively  $p_{dF}$ ). C cells also die with an increased  
855 probability  $p_{dC+}$  when the considered C cell has many other C cells in its neighborhood, in  
856 agreement with previous data (Zenke et al., 2020). Some of the probabilities are independent  
857 of the local environment ( $p_{istaF}$ ,  $p_{istaC}$ ,  $p_{iexaF}$ ,  $p_{iexaC}$ ,  $p_C$ ), the other ones being dependent  
858 of the local environment ( $p_{C/F}$ ,  $p_{dC+}$  and displacement probabilities) (Figure 6A).

859 Each simulation represents a total duration of 20 years and is divided into 3 504 000  
860 iterations, of 3 minutes each. Each type of simulation is performed 160 times. This time

861 period allowed the investigation of COPD development.. At the final state (20 years), the  
862 total numbers of F and C cells, the densities of C cells in interaction with F cells, the minimal  
863 distances between C and F cells, and the number and composition of clusters were quantified  
864 in the control and COPD situations.

865

## 866 **Statistical analyses**

867 Statistical significance, defined as  $P < 0.05$ , was analyzed by t-tests and MANOVA for  
868 variables with parametric distribution, and by Kruskal-Wallis with multiple comparison z  
869 tests, Mann-Whitney tests, Wilcoxon tests and Spearman correlation coefficients for  
870 variables with non-parametric distribution, with Graphpad Prism 6 software. RStudio  
871 software was used to perform stepwise regression and multivariate regression analyses.

872

873

874

## 875 **References**

876

- 877 Afroj, T., Mitsuhashi, A., Ogino, H., Saijo, A., Otsuka, K., Yoneda, H., Tobiume, M., Nguyen, N.  
878 T., Goto, H., Koyama, K., Sugimoto, M., Kondoh, O., Nokihara, H., & Nishioka, Y.  
879 (2021). Blockade of PD-1/PD-L1 Pathway Enhances the Antigen-Presenting Capacity of  
880 Fibrocytes. *Journal of Immunology (Baltimore, Md.: 1950)*.  
881 <https://doi.org/10.4049/jimmunol.2000909>
- 882 Backer, R. A., Hombrink, P., Helbig, C., & Amsen, D. (2018). The Fate Choice Between Effector  
883 and Memory T Cell Lineages : Asymmetry, Signal Integration, and Feedback to Create  
884 Bistability. *Advances in Immunology*, *137*, 43-82.  
885 <https://doi.org/10.1016/bs.ai.2017.12.003>
- 886 Balmelli, C., Ruggli, N., McCullough, K., & Summerfield, A. (2005). Fibrocytes are potent  
887 stimulators of anti-virus cytotoxic T cells. *Journal of Leukocyte Biology*, *77*(6), 923-933.  
888 <https://doi.org/10.1189/jlb.1204701>
- 889 Barnes, P. J. (2016). Inflammatory mechanisms in patients with chronic obstructive pulmonary  
890 disease. *The Journal of Allergy and Clinical Immunology*, *138*(1), 16-27.  
891 <https://doi.org/10.1016/j.jaci.2016.05.011>
- 892 Bertini, R., Allegretti, M., Bizzarri, C., Moriconi, A., Locati, M., Zampella, G., Cervellera, M. N.,  
893 Di Cioccio, V., Cesta, M. C., Galliera, E., Martinez, F. O., Di Bitondo, R., Troiani, G.,  
894 Sabbatini, V., D'Anniballe, G., Anacardio, R., Cutrin, J. C., Cavalieri, B., Mainiero, F., ...  
895 Colotta, F. (2004). Noncompetitive allosteric inhibitors of the inflammatory chemokine  
896 receptors CXCR1 and CXCR2 : Prevention of reperfusion injury. *Proceedings of the  
897 National Academy of Sciences of the United States of America*, *101*(32), 11791-11796.  
898 <https://doi.org/10.1073/pnas.0402090101>

- 899 Bianchetti, L., Barczyk, M., Cardoso, J., Schmidt, M., Bellini, A., & Mattoli, S. (2012).  
900 Extracellular matrix remodelling properties of human fibrocytes. *Journal of Cellular and*  
901 *Molecular Medicine*, 16(3), 483-495. <https://doi.org/10.1111/j.1582-4934.2011.01344.x>
- 902 Bivas-Benita, M., Gillard, G. O., Bar, L., White, K. A., Webby, R. J., Hovav, A.-H., & Letvin, N.  
903 L. (2013). Airway CD8 + T cells induced by pulmonary DNA immunization mediate  
904 protective anti-viral immunity. *Mucosal Immunology*, 6(1), Art. 1.  
905 <https://doi.org/10.1038/mi.2012.59>
- 906 Bucala, R., Spiegel, L. A., Chesney, J., Hogan, M., & Cerami, A. (1994). Circulating fibrocytes  
907 define a new leukocyte subpopulation that mediates tissue repair. *Molecular Medicine*  
908 *(Cambridge, Mass.)*, 1(1), 71-81.
- 909 Chang, J. T., Palanivel, V. R., Kinjyo, I., Schambach, F., Intlekofer, A. M., Banerjee, A.,  
910 Longworth, S. A., Vinup, K. E., Mrass, P., Oliaro, J., Killeen, N., Orange, J. S., Russell, S.  
911 M., Weninger, W., & Reiner, S. L. (2007). Asymmetric T lymphocyte division in the  
912 initiation of adaptive immune responses. *Science (New York, N.Y.)*, 315(5819), 1687-1691.  
913 <https://doi.org/10.1126/science.1139393>
- 914 Chang, Y., Nadigel, J., Boulais, N., Bourbeau, J., Maltais, F., Eidelman, D. H., & Hamid, Q.  
915 (2011). CD8 positive T cells express IL-17 in patients with chronic obstructive pulmonary  
916 disease. *Respiratory Research*, 12(1), 43. <https://doi.org/10.1186/1465-9921-12-43>
- 917 Chesney, J., Bacher, M., Bender, A., & Bucala, R. (1997). The peripheral blood fibrocyte is a  
918 potent antigen-presenting cell capable of priming naive T cells in situ. *Proceedings of the*  
919 *National Academy of Sciences*, 94(12), 6307-6312.  
920 <https://doi.org/10.1073/pnas.94.12.6307>
- 921 Chrysofakis, G., Tzanakis, N., Kyriakoy, D., Tsooumakidou, M., Tsiligianni, I., Klimathianaki, M.,  
922 & Siafakas, N. M. (2004). Perforin expression and cytotoxic activity of sputum CD8+  
923 lymphocytes in patients with COPD. *Chest*, 125(1), 71-76.  
924 <https://doi.org/10.1378/chest.125.1.71>
- 925 Conlon, T. M., John-Schuster, G., Heide, D., Pfister, D., Lehmann, M., Hu, Y., Ertüz, Z., Lopez,  
926 M. A., Ansari, M., Strunz, M., Mayr, C., Angelidis, I., Ciminieri, C., Costa, R., Kohlhepp,  
927 M. S., Guillot, A., Günes, G., Jeridi, A., Funk, M. C., ... Yildirim, A. Ö. (2020). Inhibition  
928 of LTβR signalling activates WNT-induced regeneration in lung. *Nature*, 588(7836),  
929 151-156. <https://doi.org/10.1038/s41586-020-2882-8>
- 930 Dayer, J.-M. (2003). How T-lymphocytes are activated and become activators by cell-cell  
931 interaction. *European Respiratory Journal*, 22(44 suppl), 10s-15s.  
932 <https://doi.org/10.1183/09031936.03.00000403b>
- 933 Dupin, I., Allard, B., Ozier, A., Maurat, E., Ousova, O., Delbrel, E., Trian, T., Bui, H.-N.,  
934 Dromer, C., Guisset, O., Blanchard, E., Hilbert, G., Vargas, F., Thumerel, M., Marthan,  
935 R., Girodet, P.-O., & Berger, P. (2016). Blood fibrocytes are recruited during acute  
936 exacerbations of chronic obstructive pulmonary disease through a CXCR4-dependent  
937 pathway. *The Journal of Allergy and Clinical Immunology*, 137(4), Art. 4.  
938 <https://doi.org/10.1016/j.jaci.2015.08.043>
- 939 Dupin, I., Contin-Bordes, C., & Berger, P. (2018). Fibrocytes in Asthma and Chronic Obstructive  
940 Pulmonary Disease : Variations on the Same Theme. *American Journal of Respiratory*  
941 *Cell and Molecular Biology*, 58(3), Art. 3. <https://doi.org/10.1165/rcmb.2017-0301PS>
- 942 Dupin I, Eyraud E, Maurat É, Sac-Épée J-M & Vallois P (2022) *Modeling cell interactions driving*  
943 *Chronic Obstructive Pulmonary Disease (COPD) via probabilistic cellular automata*  
944 (available at <https://hal.archives-ouvertes.fr/hal-03572045>).
- 945 Dupin, I., Thumerel, M., Maurat, E., Coste, F., Eyraud, E., Begueret, H., Trian, T., Montaudon,  
946 M., Marthan, R., Girodet, P.-O., & Berger, P. (2019). Fibrocyte accumulation in the  
947 airway walls of COPD patients. *The European Respiratory Journal*, 54(3), Art. 3.  
948 <https://doi.org/10.1183/13993003.02173-2018>



- 949 Dustin, M. L. (2008). T-cell activation through immunological synapses and kinapses.  
950 *Immunological Reviews*, 221, 77-89. <https://doi.org/10.1111/j.1600-065X.2008.00589.x>
- 951 Ely, K. H., Cookenham, T., Roberts, A. D., & Woodland, D. L. (2006). Memory T cell  
952 populations in the lung airways are maintained by continual recruitment. *Journal of*  
953 *Immunology (Baltimore, Md.: 1950)*, 176(1), 537-543.  
954 <https://doi.org/10.4049/jimmunol.176.1.537>
- 955 Fernando, R., Atkins, S., Raychaudhuri, N., Lu, Y., Li, B., Douglas, R. S., & Smith, T. J. (2012).  
956 Human fibrocytes coexpress thyroglobulin and thyrotropin receptor. *Proceedings of the*  
957 *National Academy of Sciences*, 109(19), 7427-7432.  
958 <https://doi.org/10.1073/pnas.1202064109>
- 959 Freeman, C. M., Curtis, J. L., & Chensue, S. W. (2007). CC chemokine receptor 5 and CXC  
960 chemokine receptor 6 expression by lung CD8+ cells correlates with chronic obstructive  
961 pulmonary disease severity. *The American Journal of Pathology*, 171(3), 767-776.  
962 <https://doi.org/10.2353/ajpath.2007.061177>
- 963 Freeman, C. M., Han, M. K., Martinez, F. J., Murray, S., Liu, L. X., Chensue, S. W., Polak, T. J.,  
964 Sonstein, J., Todt, J. C., Ames, T. M., Arenberg, D. A., Meldrum, C. A., Getty, C.,  
965 McCloskey, L., & Curtis, J. L. (2010). Cytotoxic potential of lung CD8+ T cells increases  
966 with COPD severity and with in vitro stimulation by IL-18 or IL-15. *Journal of*  
967 *immunology (Baltimore, Md. : 1950)*, 184(11), 6504-6513.  
968 <https://doi.org/10.4049/jimmunol.1000006>
- 969 Global Initiative for Chronic Obstructive Lung Disease (GOLD). Global Strategy for the Diagnosis,  
970 Management, and Prevention of Chronic Obstructive Pulmonary Disease. GOLD, 2022.  
971 Available from: <https://goldcopd.org/2022-gold-reports-2/>. Date last accessed: October 1,  
972 2022.
- 973 Gribben, J. G., Freeman, G. J., Boussiotis, V. A., Rennert, P., Jellis, C. L., Greenfield, E., Barber,  
974 M., Restivo, V. A., Ke, X., & Gray, G. S. (1995). CTLA4 mediates antigen-specific  
975 apoptosis of human T cells. *Proceedings of the National Academy of Sciences*, 92(3),  
976 811-815. <https://doi.org/10.1073/pnas.92.3.811>
- 977 Grundy, S., Plumb, J., Lea, S., Kaur, M., Ray, D., & Singh, D. (2013). Down regulation of T cell  
978 receptor expression in COPD pulmonary CD8 cells. *PloS One*, 8(8), e71629.  
979 <https://doi.org/10.1371/journal.pone.0071629>
- 980 Hayashi, H., Kawakita, A., Okazaki, S., Yasutomi, M., Murai, H., & Ohshima, Y. (2013). IL-  
981 17A/F modulates fibrocyte functions in cooperation with CD40-mediated signaling.  
982 *Inflammation*, 36(4), 830-838. <https://doi.org/10.1007/s10753-013-9609-z>
- 983 Henrot, P., Beaufils, F., Thumerel, M., Eyraud, E., Boudoussier, A., Begueret, H., Maurat, E.,  
984 Girodet, P.-O., Marthan, R., Berger, P., Dupin, I., & Zysman, M. (2021). Circulating  
985 fibrocytes as a new tool to predict lung cancer progression after surgery? *The European*  
986 *Respiratory Journal*, 2101221. <https://doi.org/10.1183/13993003.01221-2021>
- 987 Henrot, P., Eyraud, E., Maurat, E., Point, S., Cardouat, G., Quignard, J.-F., Esteves, P., Trian, T.,  
988 Girodet, P.-O., Marthan, R., Zysman, M., Berger, P., & Dupin, I. (2022). Muscarinic  
989 receptor M3 activation promotes fibrocytes contraction. *Frontiers in Pharmacology*, 13.  
990 <https://www.frontiersin.org/articles/10.3389/fphar.2022.939780>
- 991 Henrot, P., Prevel, R., Berger, P., & Dupin, I. (2019). Chemokines in COPD : From Implication to  
992 Therapeutic Use. *International Journal of Molecular Sciences*, 20(11), Art. 11.  
993 <https://doi.org/10.3390/ijms20112785>
- 994 Hodge, G., Nairn, J., Holmes, M., Reynolds, P. N., & Hodge, S. (2007). Increased intracellular T  
995 helper 1 proinflammatory cytokine production in peripheral blood, bronchoalveolar lavage  
996 and intraepithelial T cells of COPD subjects. *Clinical and Experimental Immunology*,  
997 150(1), 22-29. <https://doi.org/10.1111/j.1365-2249.2007.03451.x>

- 998 Hogg, J. C., Chu, F., Utokaparch, S., Woods, R., Elliott, W. M., Buzatu, L., Cherniack, R. M.,  
999 Rogers, R. M., Sciurba, F. C., Coxson, H. O., & Paré, P. D. (2004). The nature of small-  
1000 airway obstruction in chronic obstructive pulmonary disease. *The New England Journal of*  
1001 *Medicine*, 350(26), 2645-2653. <https://doi.org/10.1056/NEJMoa032158>
- 1002 Hogg, J. C., Williams, J., Richardson, J. B., Macklem, P. T., & Thurlbeck, W. M. (1970). Age as  
1003 a Factor in the Distribution of Lower-Airway Conductance and in the Pathologic Anatomy  
1004 of Obstructive Lung Disease. *New England Journal of Medicine*, 282(23), 1283-1287.  
1005 <https://doi.org/10.1056/NEJM197006042822302>
- 1006 Hombrink, P., Helbig, C., Backer, R. A., Piet, B., Oja, A. E., Stark, R., Brassler, G., Jongejan, A.,  
1007 Jonkers, R. E., Nota, B., Basak, O., Clevers, H. C., Moerland, P. D., Amsen, D., &  
1008 van Lier, R. A. W. (2016). Programs for the persistence, vigilance and control of human  
1009 CD8+ lung-resident memory T cells. *Nature Immunology*, 17(12), 1467-1478.  
1010 <https://doi.org/10.1038/ni.3589>
- 1011 Hufford, M. M., Kim, T. S., Sun, J., & Braciale, T. J. (2011). Antiviral CD8+ T cell effector  
1012 activities in situ are regulated by target cell type. *The Journal of Experimental Medicine*,  
1013 208(1), 167-180. <https://doi.org/10.1084/jem.20101850>
- 1014 Hurst, J. R., Vestbo, J., Anzueto, A., Locantore, N., Müllerova, H., Tal-Singer, R., Miller, B.,  
1015 Lomas, D. A., Agustí, A., Macnee, W., Calverley, P., Rennard, S., Wouters, E. F. M.,  
1016 Wedzicha, J. A., & Evaluation of COPD Longitudinally to Identify Predictive Surrogate  
1017 Endpoints (ECLIPSE) Investigators. (2010). Susceptibility to exacerbation in chronic  
1018 obstructive pulmonary disease. *The New England Journal of Medicine*, 363(12),  
1019 1128-1138. <https://doi.org/10.1056/NEJMoa0909883>
- 1020 Kaur, M., Smyth, L. J., Cadden, P., Grundy, S., Ray, D., Plumb, J., & Singh, D. (2012). T  
1021 lymphocyte insensitivity to corticosteroids in chronic obstructive pulmonary disease.  
1022 *Respiratory Research*, 13, 20. <https://doi.org/10.1186/1465-9921-13-20>
- 1023 Lethbridge, M. W., Kemeny, D. M., Ratoff, J. C., O'Connor, B. J., Hawrylowicz, C. M., &  
1024 Corrigan, C. J. (2010). A novel technique to explore the functions of bronchial mucosal T  
1025 cells in chronic obstructive pulmonary disease : Application to cytotoxicity and cytokine  
1026 immunoreactivity. *Clinical and Experimental Immunology*, 161(3), 560-569.  
1027 <https://doi.org/10.1111/j.1365-2249.2010.04198.x>
- 1028 Ling, C., Nishimoto, K., Rolfs, Z., Smith, L. M., Frey, B. L., & Welham, N. V. (2019).  
1029 Differentiated fibrocytes assume a functional mesenchymal phenotype with regenerative  
1030 potential. *Science Advances*, 5(5), eaav7384. <https://doi.org/10.1126/sciadv.aav7384>
- 1031 Løkke, A., Lange, P., Scharling, H., Fabricius, P., & Vestbo, J. (2006). Developing COPD : A 25  
1032 year follow up study of the general population. *Thorax*, 61(11), 935-939.  
1033 <https://doi.org/10.1136/thx.2006.062802>
- 1034 Lundblad, L. K. A., Thompson-Figueroa, J., Leclair, T., Sullivan, M. J., Poynter, M. E., Irvin, C.  
1035 G., & Bates, J. H. T. (2005). Tumor Necrosis Factor- $\alpha$  Overexpression in Lung Disease.  
1036 *American Journal of Respiratory and Critical Care Medicine*, 171(12), 1363-1370.  
1037 <https://doi.org/10.1164/rccm.200410-1349OC>
- 1038 Mackay, C. R. (2001). Chemokines : Immunology's high impact factors. *Nature Immunology*,  
1039 2(2), 95-101. <https://doi.org/10.1038/84298>
- 1040 Maeno, T., Houghton, A. M., Quintero, P. A., Grumelli, S., Owen, C. A., & Shapiro, S. D. (2007).  
1041 CD8+ T Cells are required for inflammation and destruction in cigarette smoke-induced  
1042 emphysema in mice. *Journal of Immunology (Baltimore, Md.: 1950)*, 178(12), 8090-8096.  
1043 <https://doi.org/10.4049/jimmunol.178.12.8090>
- 1044 Mannino, D. M., & Buist, A. S. (2007). Global burden of COPD : Risk factors, prevalence, and  
1045 future trends. *Lancet (London, England)*, 370(9589), 765-773.  
1046 [https://doi.org/10.1016/S0140-6736\(07\)61380-4](https://doi.org/10.1016/S0140-6736(07)61380-4)



- 1047 McKendry, R. T., Spalluto, C. M., Burke, H., Nicholas, B., Cellura, D., Al-Shamkhani, A.,  
1048 Staples, K. J., & Wilkinson, T. M. A. (2016). Dysregulation of Antiviral Function of  
1049 CD8+ T Cells in the Chronic Obstructive Pulmonary Disease Lung. Role of the PD-1–PD-  
1050 L1 Axis. *American Journal of Respiratory and Critical Care Medicine*, *193*(6), 642-651.  
1051 <https://doi.org/10.1164/rccm.201504-0782OC>
- 1052 McMaster, S. R., Wilson, J. J., Wang, H., & Kohlmeier, J. E. (2015). Airway-Resident Memory  
1053 CD8 T Cells Provide Antigen-Specific Protection against Respiratory Virus Challenge  
1054 through Rapid IFN- $\gamma$  Production. *Journal of Immunology (Baltimore, Md.: 1950)*, *195*(1),  
1055 203-209. <https://doi.org/10.4049/jimmunol.1402975>
- 1056 Mead, J. (1970). The Lung's Quiet Zone. *New England Journal of Medicine*, *282*(23), 1318-1319.  
1057 <https://doi.org/10.1056/NEJM197006042822311>
- 1058 Miller, M. J., Hejazi, A. S., Wei, S. H., Cahalan, M. D., & Parker, I. (2004). T cell repertoire  
1059 scanning is promoted by dynamic dendritic cell behavior and random T cell motility in the  
1060 lymph node. *Proceedings of the National Academy of Sciences of the United States of*  
1061 *America*, *101*(4), 998-1003. <https://doi.org/10.1073/pnas.0306407101>
- 1062 Moreau, H. D., Lemaître, F., Terriac, E., Azar, G., Piel, M., Lennon-Dumenil, A.-M., & Bousso,  
1063 P. (2012). Dynamic in situ cytometry uncovers T cell receptor signaling during  
1064 immunological synapses and kinapses in vivo. *Immunity*, *37*(2), 351-363.  
1065 <https://doi.org/10.1016/j.immuni.2012.05.014>
- 1066 Morissette, M. C., Parent, J., & Milot, J. (2007). Perforin, granzyme B, and FasL expression by  
1067 peripheral blood T lymphocytes in emphysema. *Respiratory Research*, *8*(1), 62.  
1068 <https://doi.org/10.1186/1465-9921-8-62>
- 1069 Mrass, P., Oruganti, S. R., Fricke, G. M., Tafoya, J., Byrum, J. R., Yang, L., Hamilton, S. L.,  
1070 Miller, M. J., Moses, M. E., & Cannon, J. L. (2017). ROCK regulates the intermittent  
1071 mode of interstitial T cell migration in inflamed lungs. *Nature Communications*, *8*(1),  
1072 1010. <https://doi.org/10.1038/s41467-017-01032-2>
- 1073 Mukhopadhyay, S., Hoidal, J. R., & Mukherjee, T. K. (2006). Role of TNFalpha in pulmonary  
1074 pathophysiology. *Respiratory Research*, *7*, 125. <https://doi.org/10.1186/1465-9921-7-125>
- 1075 Nemzek, J. A., Fry, C., & Moore, B. B. (2013). Adoptive transfer of fibrocytes enhances splenic  
1076 T-cell numbers and survival in septic peritonitis. *Shock (Augusta, Ga.)*, *40*(2), 106-114.  
1077 <https://doi.org/10.1097/SHK.0b013e31829c3c68>
- 1078 Ngo, V. N., Tang, H. L., & Cyster, J. G. (1998). Epstein-Barr virus-induced molecule 1 ligand  
1079 chemokine is expressed by dendritic cells in lymphoid tissues and strongly attracts naive T  
1080 cells and activated B cells. *The Journal of Experimental Medicine*, *188*(1), 181-191.  
1081 <https://doi.org/10.1084/jem.188.1.181>
- 1082 Niedermeier, M., Reich, B., Rodriguez Gomez, M., Denzel, A., Schmidbauer, K., Göbel, N.,  
1083 Talke, Y., Schweda, F., & Mack, M. (2009). CD4+ T cells control the differentiation of  
1084 Gr1+ monocytes into fibrocytes. *Proceedings of the National Academy of Sciences of the*  
1085 *United States of America*, *106*(42), 17892-17897.  
1086 <https://doi.org/10.1073/pnas.0906070106>
- 1087 Obst, R. (2015). The Timing of T Cell Priming and Cycling. *Frontiers in Immunology*, *6*.  
1088 <https://www.frontiersin.org/article/10.3389/fimmu.2015.00563>
- 1089 O'Shaughnessy, T. C., Ansari, T. W., Barnes, N. C., & Jeffery, P. K. (1997). Inflammation in  
1090 bronchial biopsies of subjects with chronic bronchitis : Inverse relationship of CD8+ T  
1091 lymphocytes with FEV1. *American Journal of Respiratory and Critical Care Medicine*,  
1092 *155*(3), 852-857. <https://doi.org/10.1164/ajrccm.155.3.9117016>
- 1093 Pilling, D., Zheng, Z., Vakil, V., & Gomer, R. H. (2014). Fibroblasts secrete Slit2 to inhibit  
1094 fibrocyte differentiation and fibrosis. *Proceedings of the National Academy of Sciences*,  
1095 *111*(51), 18291-18296. <https://doi.org/10.1073/pnas.1417426112>

- 1096 Pothen, J. J., Poynter, M. E., & Bates, J. H. T. (2015). A computational model of unresolved  
1097 allergic inflammation in chronic asthma. *American Journal of Physiology - Lung Cellular*  
1098 *and Molecular Physiology*, 308(4), L384-L390.  
1099 <https://doi.org/10.1152/ajplung.00268.2014>
- 1100 Roos-Engstrand, E., Ekstrand-Hammarström, B., Pourazar, J., Behndig, A. F., Bucht, A., &  
1101 Blomberg, A. (2009). Influence of smoking cessation on airway T lymphocyte subsets in  
1102 COPD. *COPD*, 6(2), 112-120. <https://doi.org/10.1080/15412550902755358>
- 1103 Saetta, M., Baraldo, S., Corbino, L., Turato, G., Braccioni, F., Rea, F., Cavallese, G., Tropeano,  
1104 G., Mapp, C. E., Maestrelli, P., Ciaccia, A., & Fabbri, L. M. (1999). CD8+ve cells in the  
1105 lungs of smokers with chronic obstructive pulmonary disease. *American Journal of*  
1106 *Respiratory and Critical Care Medicine*, 160(2), 711-717.  
1107 <https://doi.org/10.1164/ajrccm.160.2.9812020>
- 1108 Saetta, M., Di STEFANO, A., Turato, G., Facchini, F. M., Corbino, L., Mapp, C. E., Maestrelli,  
1109 P., Ciaccia, A., & Fabbri, L. M. (1998). CD8+ T-Lymphocytes in Peripheral Airways of  
1110 Smokers with Chronic Obstructive Pulmonary Disease. *American Journal of Respiratory*  
1111 *and Critical Care Medicine*, 157(3), 822-826.  
1112 <https://doi.org/10.1164/ajrccm.157.3.9709027>
- 1113 Saunders, R., Kaul, H., Berair, R., Gonem, S., Singapuri, A., Sutcliffe, A. J., Chachi, L., Biddle,  
1114 M. S., Kaur, D., Bourne, M., Pavord, I. D., Wardlaw, A. J., Siddiqui, S. H., Kay, R. A.,  
1115 Brook, B. S., Smallwood, R. H., & Brightling, C. E. (2019). DP2 antagonism reduces  
1116 airway smooth muscle mass in asthma by decreasing eosinophilia and myofibroblast  
1117 recruitment. *Science Translational Medicine*, 11(479), Art. 479.  
1118 <https://doi.org/10.1126/scitranslmed.aa06451>
- 1119 Scheipers, P., & Reiser, H. (1998). Fas-independent death of activated CD4+ T lymphocytes  
1120 induced by CTLA-4 crosslinking. *Proceedings of the National Academy of Sciences*,  
1121 95(17), 10083-10088. <https://doi.org/10.1073/pnas.95.17.10083>
- 1122 Schmidt, M., Sun, G., Stacey, M. A., Mori, L., & Mattoli, S. (2003). Identification of circulating  
1123 fibrocytes as precursors of bronchial myofibroblasts in asthma. *Journal of Immunology*  
1124 *(Baltimore, Md.: 1950)*, 171(1), 380-389. <https://doi.org/10.4049/jimmunol.171.1.380>
- 1125 Schneider, C. A., Rasband, W. S., & Eliceiri, K. W. (2012). NIH Image to ImageJ : 25 years of  
1126 image analysis. *Nature Methods*, 9(7), Art. 7. <https://doi.org/10.1038/nmeth.2089>
- 1127 Schyns, J., Bai, Q., Ruscitti, C., Radermecker, C., De Schepper, S., Chakarov, S., Farnir, F.,  
1128 Pirottin, D., Ginhoux, F., Boeckxstaens, G., Bureau, F., & Marichal, T. (2019). Non-  
1129 classical tissue monocytes and two functionally distinct populations of interstitial  
1130 macrophages populate the mouse lung. *Nature Communications*, 10(1), 3964.  
1131 <https://doi.org/10.1038/s41467-019-11843-0>
- 1132 Siena, L., Gjomarkaj, M., Elliot, J., Pace, E., Bruno, A., Baraldo, S., Saetta, M., Bonsignore, M.  
1133 R., & James, A. (2011). Reduced apoptosis of CD8+ T-lymphocytes in the airways of  
1134 smokers with mild/moderate COPD. *Respiratory Medicine*, 105(10), 1491-1500.  
1135 <https://doi.org/10.1016/j.rmed.2011.04.014>
- 1136 Takamura, S., Kato, S., Motozono, C., Shimaoka, T., Ueha, S., Matsuo, K., Miyauchi, K.,  
1137 Masumoto, T., Katsushima, A., Nakayama, T., Tomura, M., Matsushima, K., Kubo, M., &  
1138 Miyazawa, M. (2019). Interstitial-resident memory CD8+ T cells sustain frontline  
1139 epithelial memory in the lung. *Journal of Experimental Medicine*, 216(12), 2736-2747.  
1140 <https://doi.org/10.1084/jem.20190557>
- 1141 Takamura, S., Yagi, H., Hakata, Y., Motozono, C., McMaster, S. R., Masumoto, T., Fujisawa, M.,  
1142 Chikaishi, T., Komeda, J., Itoh, J., Umemura, M., Kyusai, A., Tomura, M., Nakayama, T.,  
1143 Woodland, D. L., Kohlmeier, J. E., & Miyazawa, M. (2016). Specific niches for lung-  
1144 resident memory CD8+ T cells at the site of tissue regeneration enable CD69-independent

- 1145 maintenance. *The Journal of Experimental Medicine*, 213(13), 3057-3073.  
1146 <https://doi.org/10.1084/jem.20160938>
- 1147 Velotti, F., Barchetta, I., Cimini, F. A., & Cavallo, M. G. (2020). Granzyme B in Inflammatory  
1148 Diseases : Apoptosis, Inflammation, Extracellular Matrix Remodeling, Epithelial-to-  
1149 Mesenchymal Transition and Fibrosis. *Frontiers in Immunology*, 11, 587581.  
1150 <https://doi.org/10.3389/fimmu.2020.587581>
- 1151 von Andrian, U. H., & Mackay, C. R. (2000). T-cell function and migration. Two sides of the  
1152 same coin. *The New England Journal of Medicine*, 343(14), 1020-1034.  
1153 <https://doi.org/10.1056/NEJM200010053431407>
- 1154 Wang, X., Zhang, D., Higham, A., Wolosianka, S., Gai, X., Zhou, L., Petersen, H., Pinto-Plata,  
1155 V., Divo, M., Silverman, E. K., Celli, B., Singh, D., Sun, Y., & Owen, C. A. (2020).  
1156 ADAM15 expression is increased in lung CD8+ T cells, macrophages, and bronchial  
1157 epithelial cells in patients with COPD and is inversely related to airflow obstruction.  
1158 *Respiratory Research*, 21(1), 188. <https://doi.org/10.1186/s12931-020-01446-5>
- 1159 Williamson, B. D., Carswell, E. A., Rubin, B. Y., Prendergast, J. S., & Old, L. J. (1983). Human  
1160 tumor necrosis factor produced by human B-cell lines : Synergistic cytotoxic interaction  
1161 with human interferon. *Proceedings of the National Academy of Sciences*, 80(17),  
1162 5397-5401. <https://doi.org/10.1073/pnas.80.17.5397>
- 1163 Wright, J. L., Tai, H., Wang, R., Wang, X., & Churg, A. (2007). Cigarette smoke upregulates  
1164 pulmonary vascular matrix metalloproteinases via TNF-alpha signaling. *American Journal  
1165 of Physiology. Lung Cellular and Molecular Physiology*, 292(1), L125-133.  
1166 <https://doi.org/10.1152/ajplung.00539.2005>
- 1167 Xu, F., Vasilescu, D. M., Kinose, D., Tanabe, N., Ng, K. W., Coxson, H. O., Cooper, J. D.,  
1168 Hackett, T.-L., Verleden, S. E., Vanaudenaerde, B. M., Stevenson, C. S., Lenburg, M. E.,  
1169 Spira, A., Tan, W. C., Sin, D. D., Ng, R. T., & Hogg, J. C. (2021). The molecular and  
1170 cellular mechanisms associated with the destruction of terminal bronchioles in chronic  
1171 obstructive pulmonary disease. *European Respiratory Journal*.  
1172 <https://doi.org/10.1183/13993003.01411-2021>
- 1173 Zenke, S., Palm, M. M., Braun, J., Gavrillov, A., Meiser, P., Böttcher, J. P., Beyersdorf, N., Ehl,  
1174 S., Gerard, A., Lämmermann, T., Schumacher, T. N., Beltman, J. B., & Rohr, J. C. (2020).  
1175 Quorum Regulation via Nested Antagonistic Feedback Circuits Mediated by the Receptors  
1176 CD28 and CTLA-4 Confers Robustness to T Cell Population Dynamics. *Immunity*, 52(2),  
1177 313-327.e7. <https://doi.org/10.1016/j.immuni.2020.01.018>  
1178

1179 **Acknowledgments**

1180 We thank the study participants and the staff of the Thoracic Surgery, Radiology, Pathology,  
1181 Respiratory, Lung Function Testing departments from the University Hospital of Bordeaux  
1182 (Bordeaux, France), Isabelle Goasdoue, Isabelle Bernis, Natacha Robert, Virginie Niel, and  
1183 Marine Servat from the clinical investigation center for technical assistance, and Atika  
1184 Zouine and Vincent Pitard for technical assistance at the Flow cytometry facility (CNRS  
1185 UMS 3427, INSERM US 005, Univ. Bordeaux, F-33000 Bordeaux, France), Christel  
1186 Poujol, Sébastien Marais and Fabrice Cordelières for help with imaging and image analysis  
1187 et the Bordeaux Imaging Centre (BIC; Bordeaux, France). Microscopy was performed at  
1188 BIC, a service unit of the CNRS-INSERM and Bordeaux University, a member of the  
1189 national BioImaging infrastructure of France supported by the French National Research  
1190 Agency (ANR-10-INBS-04).

1191

1192 **Funding:** The project was funded by :

1193 the “Fondation de l’Université de Bordeaux” (Fonds pour les maladies chroniques  
1194 nécessitant une assistance médico-technique FGLMR/AVAD) (ID)

1195 the “Agence Nationale de la Recherche” (ANR-21-CE18-0001-01) (ID)

1196 AstraZeneca (an unrestricted grant to PB).

1197 The COBRA cohort was funded by AstraZeneca, Chiesi, Glaxo-SmithKline, Novartis and

1198 Roche.

1199

1200 **Author contributions:**

1201 Conceptualization: PV, CCB, PB, ID

1202 Methodology: EE, EM, PH, MZ, HB, POG, MT, RHC, FL, PV, CCB, PB, ID

1203 Software: JMSE, PV, FL

1204 Formal analysis: EE, EM, JMSE, PV, ID

1205 Investigation: EE, EM, JMSE, PH, MZ, PE, TT, MT, RHC, PV, CCB, ID

1206 Visualization: EE, EM, JMSE, PH, ID

1207 Supervision: ID

1208 Writing—original draft: EE, ID

Writing—review & editing: EE, PH, RM, PV, CCB, PB, ID

1209  
1210

1211 **Competing interests:** PB, POG, ID have a patent (EP N°3050574: Use of plerixafor for treating  
1212 and/or preventing acute exacerbations of chronic obstructive pulmonary disease) granted.  
1213 MZ reports personal fees from AstraZeneca, Boehringer Ingelheim, Novartis, Chiesi,  
1214 GlaxoSmithKline and non-financial support Lilly outside the submitted work; POG reports  
1215 grants, personal fees and non-financial support from AstraZeneca, personal fees and non-  
1216 financial support from Chiesi, personal fees and non-financial support from  
1217 GlaxoSmithKline, personal fees and non-financial support from Novartis, personal fees and  
1218 non-financial support from Sanofi, outside the submitted work; PB reports grants from  
1219 AstraZeneca, Glaxo-Smith-Kline, Novartis, Chiesi, which support COBRA during the  
1220 conduct of the study; grants and personal fees from AstraZeneca, BoehringerIngelheim,  
1221 Novartis, personal fees and non-financial support from Chiesi, Sanofi, Menarini, outside the  
1222 submitted work; ID, MZ and PH report grants from the “Fondation Bordeaux Université,”  
1223 with funding from "Assistance Ventilatoire à Domicile" (AVAD) and "Fédération  
1224 Girondine de Lutte contre les Maladies Respiratoires" (FGLMR) during the conduct of the  
1225 study. All other authors declare they have no competing interests.  
1226

1227 **Data and materials availability:** All data needed to evaluate the conclusions are present  
1228 in the paper, the Supplementary Materials, and/or the deposited data. The customized  
1229 ImageJ plugin used to perform Delaunay triangulation and cluster quantification is available  
1230 here:

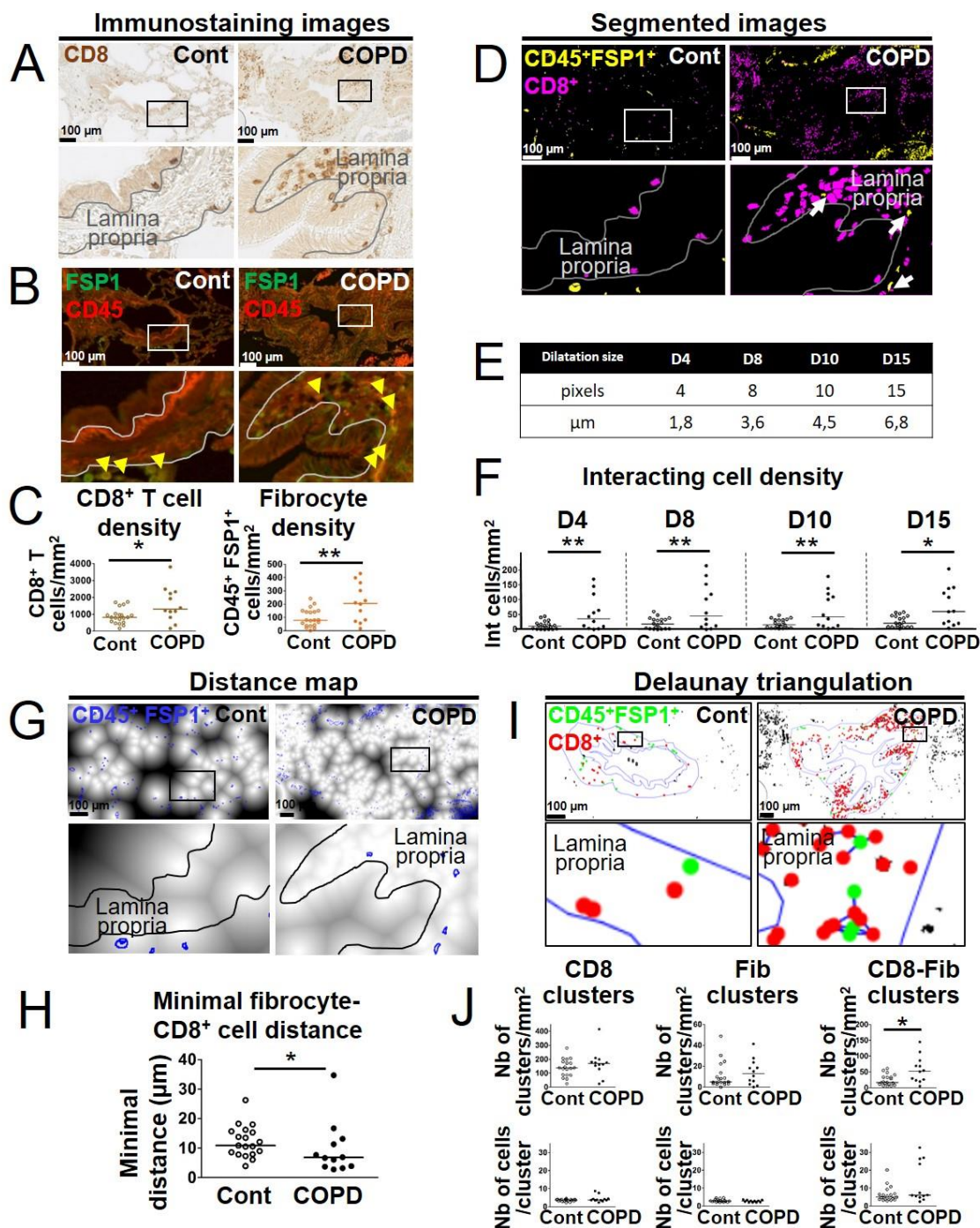
1231 [https://github.com/fle vet/Delaunay\\_clustering\\_ImageJ](https://github.com/fle vet/Delaunay_clustering_ImageJ)

1232 A complete version of the code for launching the simulations associated to control and  
1233 COPD dynamics can be downloaded from the following site:

1234 <https://plmbox.math.cnrs.fr/d/49bcbc1db63a4654be7e/>



1235 **Figures**  
1236



1237  
1238  
1239  
1240  
1241  
1242  
1243  
1244  
1245  
1246  
1247

**Figure 1. Increased interactions between CD8<sup>+</sup> T cells, CD45<sup>+</sup> FSP1<sup>+</sup> cells in distal airways of COPD patients.** (A, B) Representative stainings of CD8 (brown, A), CD45 (red, B) and FSP1 (green, B) in distal bronchial tissue specimens from a control subject (left) and a COPD patient (right). The yellow arrowheads indicate fibrocytes, defined as CD45<sup>+</sup> FSP1<sup>+</sup> cells. (C) Quantification of CD8<sup>+</sup> T cells and fibrocyte densities (normalized by the sub-epithelial area) in one specimen/patient. (D) Merged segmented images for CD8 and CD45-FSP1 staining, showing CD8<sup>+</sup> T cells and CD45<sup>+</sup> FSP1<sup>+</sup> cells respectively in magenta and yellow. The white arrows indicate interacting cells, detected by dilatation of CD8 positive particle. (E) Table showing the correspondence between dilatations in pixels and  $\mu$ m. F, Quantification of interacting cells densities (normalized by the sub-epithelial area) in one

1248 specimen/patient, using the different dilatations sizes (**E**). (**G**) Distance maps built from the  
1249 binary image produced from CD8 staining, with FSP1<sup>+</sup> CD45<sup>+</sup> cells (blue outlines). (**H**)  
1250 Quantification of the mean minimal distances between fibrocyte and CD8<sup>+</sup> T cells in one  
1251 specimen/patient. (**I**) Cluster analysis performed by Delaunay triangulation on segmented  
1252 images for CD8 and CD45-FSP1 staining, followed by the application of a threshold value  
1253 (40  $\mu\text{m}$ ) above which connections are not kept. CD8<sup>+</sup> T cells and fibrocytes appear  
1254 respectively with green and red dots, connections are shown in blue. (**J**) First row: densities  
1255 of clusters containing exclusively CD8<sup>+</sup> T cells (“CD8 clusters”), fibrocytes (“Fib clusters”)  
1256 and both cell types (“CD8-Fib clusters”) normalized by the sub-epithelial area) in one  
1257 specimen/patient. Second row: mean number of cells by cluster. (**C, F, H, J**) The medians  
1258 are represented as horizontal lines. \*: P<0.05, \*\*:P<0.01; \*\*\*: P<0.001. unpaired t-tests or  
1259 Mann Whitney tests.

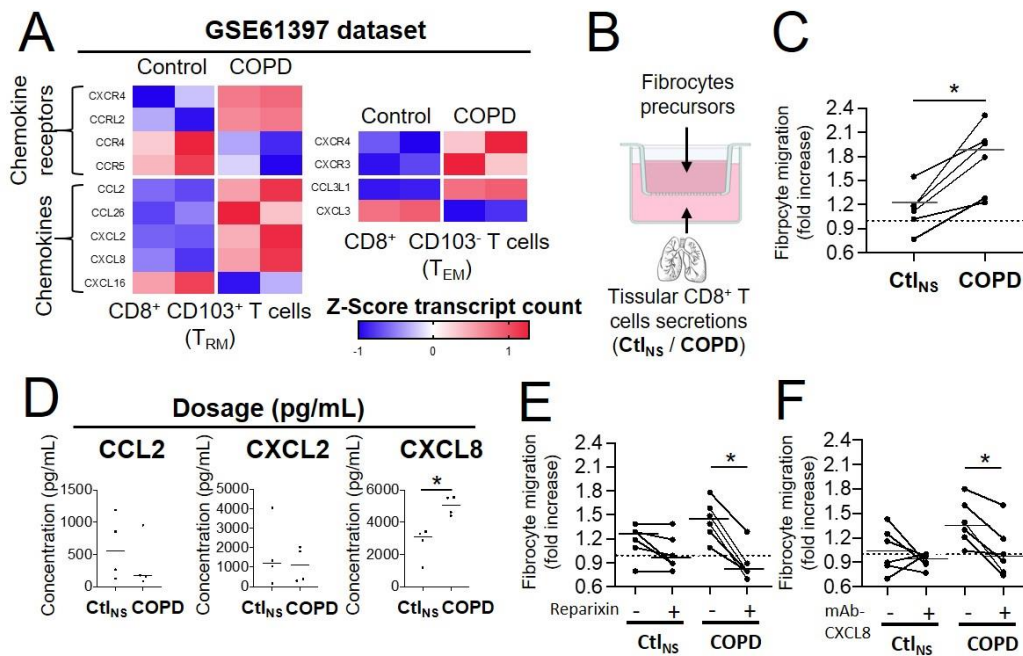


**Figure 2. CD8<sup>+</sup> T cells from COPD tissue have increased chemoattractive properties for fibrocytes.** (A) Heatmaps showing the expression of differentially expressed genes with p-value<0.05 of chemokines and chemokine receptors in resting tissular tissue resident memory T-cells (T<sub>RM</sub>) and effector memory T-cells (T<sub>EM</sub>) from patients with COPD (n=2 independent samples) in comparison with control subjects (n=2 independent samples) (GEO accession GSE61397). Expression values are expressed as Z-score transformed transcript count. (B) Migration experiment design. (C) Migration of fibrocytes from patients with COPD in response to CD8<sup>+</sup> T cells supernatants from control subjects (Ctl<sub>NS</sub>) or COPD patients (COPD). (D) CCL2, CXCL2 and CXCL8 levels in CD8<sup>+</sup> T cells supernatants from non-smoking control subjects (Ctl<sub>NS</sub>) or patients with COPD (COPD) using BioPlex (CCL2, CXCL2) or ELISA (CXCL8). \* P < 0.05, Mann–Whitney test. (E-F), Migration of fibrocytes from patients with COPD in response to CD8<sup>+</sup> T cells supernatants from control subjects (Ctl<sub>NS</sub>) or COPD patients (COPD), in the presence of 200nM Reparixin (+) or corresponding vehicle (-) (E), and in the presence of 1μg/mL blocking antibody for CXCL8 (+) or control antibody (-) (F). \* P < 0.05, Wilcoxon matched pairs test.

1260  
1261  
1262  
1263  
1264  
1265  
1266  
1267  
1268  
1269  
1270  
1271  
1272  
1273  
1274  
1275



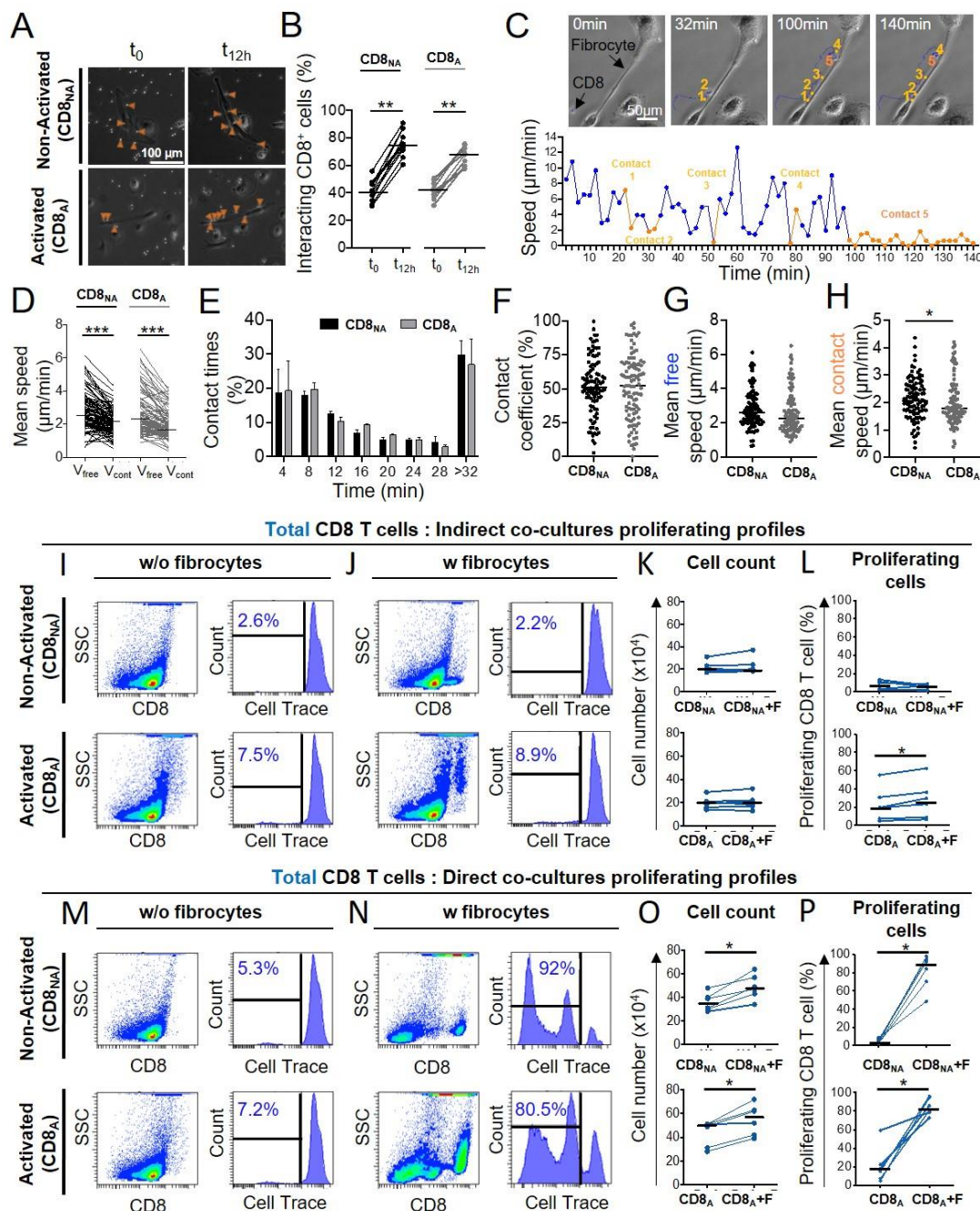


**Figure 3. CD8<sup>+</sup> T cell repeatedly contact fibrocytes and this contact greatly enhances CD8<sup>+</sup> T cell proliferation.** Prior to co-culture, CD8<sup>+</sup> T cells have been either non-activated (“CD8<sub>NA</sub>”) or activated (“CD8<sub>A</sub>”). (A) Representative brightfield images of co-culture between CD8<sup>+</sup> T cells and fibrocytes at the initial state of the acquisition (t<sub>0</sub>) and after 12 hours (t<sub>12h</sub>) in both conditions of activation. The orange arrowheads indicate CD8<sup>+</sup> T cells (bright round-shaped cells) in contact with fibrocytes (elongated adherent cells). (B) Quantifications of the proportion of fibrocyte-interacting CD8<sup>+</sup> T cells at t<sub>0</sub> and t<sub>12h</sub> in both conditions of activation. (C) Top panel: typical CD8<sup>+</sup> T cells trajectory (blue) relatively to a fibrocyte (elongated adherent cell) for a period of 140 min. Bottom panel: speed (μm/min) over time for the tracked CD8<sup>+</sup> T cell. Short-lived (<12 min, n=4) and longer-lived (>32 min, n=1) contacts are represented respectively in light and dark orange. (D) Comparison of the mean speed of individual CD8<sup>+</sup> T cells measured in the absence (“V<sub>free</sub>”) or presence (“V<sub>cont</sub>”) of contact with fibrocytes in both conditions of activation. (E) Mean frequency

1276  
1277  
1278  
1279  
1280  
1281  
1282  
1283  
1284  
1285  
1286  
1287  
1288  
1289  
1290

1291 distributions of contact time duration (with 4 min binning) between CD8<sup>+</sup> T cells and  
1292 fibrocytes for CD8<sub>NA</sub> (black) and CD8<sub>A</sub> (gray). Error bars indicate standard error of the  
1293 mean. **(F-H)** Dot plots representing spatiotemporal variables measured for each individual  
1294 CD8<sup>+</sup> T cell tracked over 12h. Each dot represents one cell. **(F)** Contact coefficient. **(G)**  
1295 Mean speed of CD8<sup>+</sup> T cells measured in the absence of contact with fibrocytes (“Mean free  
1296 speed”). **(H)** Mean speed of CD8<sup>+</sup> T cells measured in the presence of contact with  
1297 fibrocytes (“Mean contact speed”). **(I, J, M, N)** Representative gating strategy for  
1298 identification of CD8<sup>+</sup> T cells without (w/o) fibrocytes **(I, M)** or with (w) fibrocytes **(J, N)**  
1299 in indirect **(I, J)** or direct **(M, N)** co-culture. Left panels: dot plots represent representative  
1300 CD8-PerCP-Cy5-5 fluorescence (y-axis) versus side scatter (SSC, x-axis) of non-adherent  
1301 cells removed from the culture. Right panels: histograms represent representative cell count  
1302 (y-axis) versus Cell Trace-Pacific Blue fluorescence (x-axis). The distinct fluorescence  
1303 peaks correspond to the different generations of CD8<sup>+</sup> T cells. The gate and the percentage  
1304 indicate cells that have proliferated. **(K, O)** Comparison of manual count of non-adherent  
1305 cells removed from co-culture without fibrocyte (“CD8”) and with fibrocyte (“CD8+F”). **L,**  
1306 **(P)** Comparison of quantifications of CD8<sup>+</sup> T cells that have proliferated, removed from co-  
1307 culture without fibrocyte (“CD8”) and with fibrocyte (“CD8+F”). **(B, D, F, G, H, K, L, O,**  
1308 **P)** Medians are represented as horizontal lines. \* P < 0.05, \*\* P < 0.01, \*\*\* P < 0.001. **(B,**  
1309 **D, K, L, O, P)** Wilcoxon matched pairs test. **(F, G, H)** Mann Whitney tests.

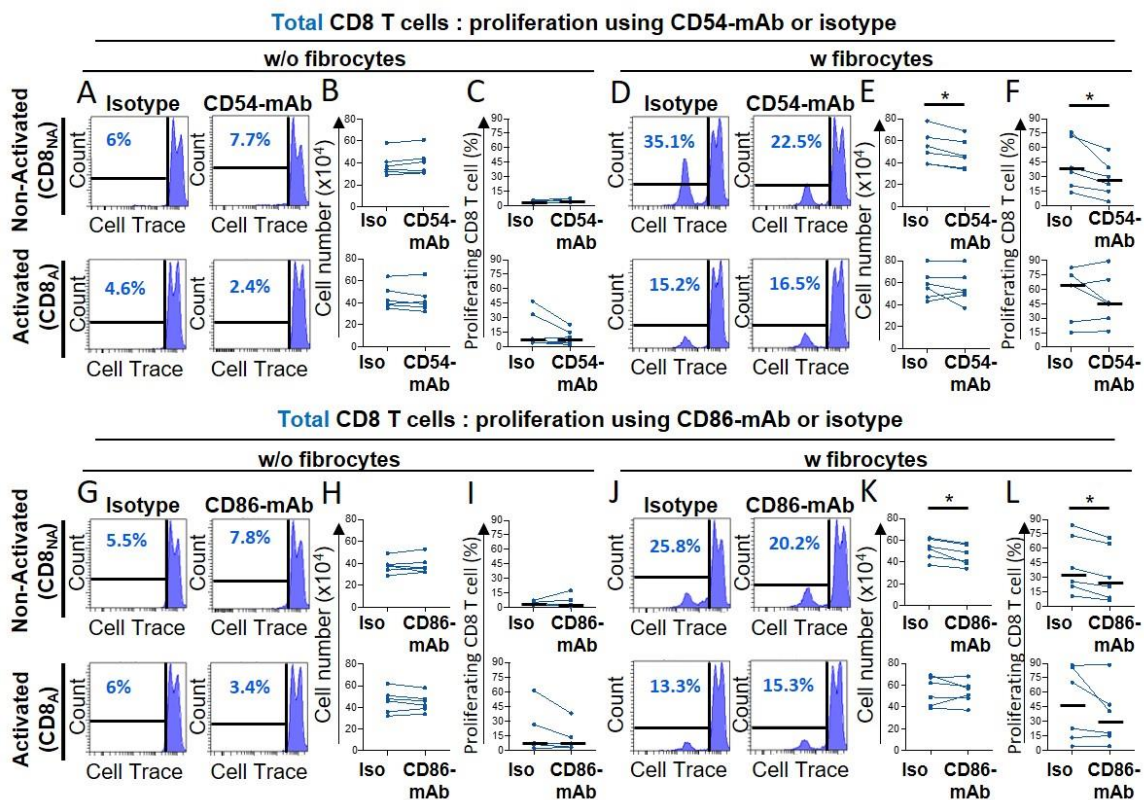


**Figure 4. Fibrocytes act as a major promoter on CD8<sup>+</sup> T cell proliferation in a CD54 and CD86-dependent manner.** Prior to co-culture, CD8<sup>+</sup> T cells have been either non-activated (“CD8<sub>NA</sub>”) or activated (“CD8<sub>A</sub>”). (A, D, G, J) Representative gating strategy for identification of proliferating CD8<sup>+</sup> T cells without (w/o) fibrocytes (A, G) or with (w) fibrocytes (D, J) using neutralizing CD54-mAb (A, D) or neutralizing CD86-mAb (G, J) and respective control isotype. Histograms represent representative cell count (y-axis) versus Cell Trace-Pacific Blue fluorescence (x-axis). The distinct fluorescence peaks correspond to the different generations of CD8<sup>+</sup> T cells. The gate and the percentage indicate cells that have proliferated. (B, E, H, K) Comparison of manual count of non-adherent cells removed from co-culture treated with neutralizing CD54-mAb or control isotype (Iso) (B, E) and neutralizing CD86-mAb or control isotype (Iso) (H, K). (C, F, I, L) Comparison of quantifications of CD8<sup>+</sup> T cells that have proliferated, removed from co-culture treated with neutralizing CD54-mAb (C, F) or neutralizing CD86-mAb (I, L) and respective control isotype. Medians are represented as horizontal lines. \* P < 0.05, Wilcoxon matched pairs test.



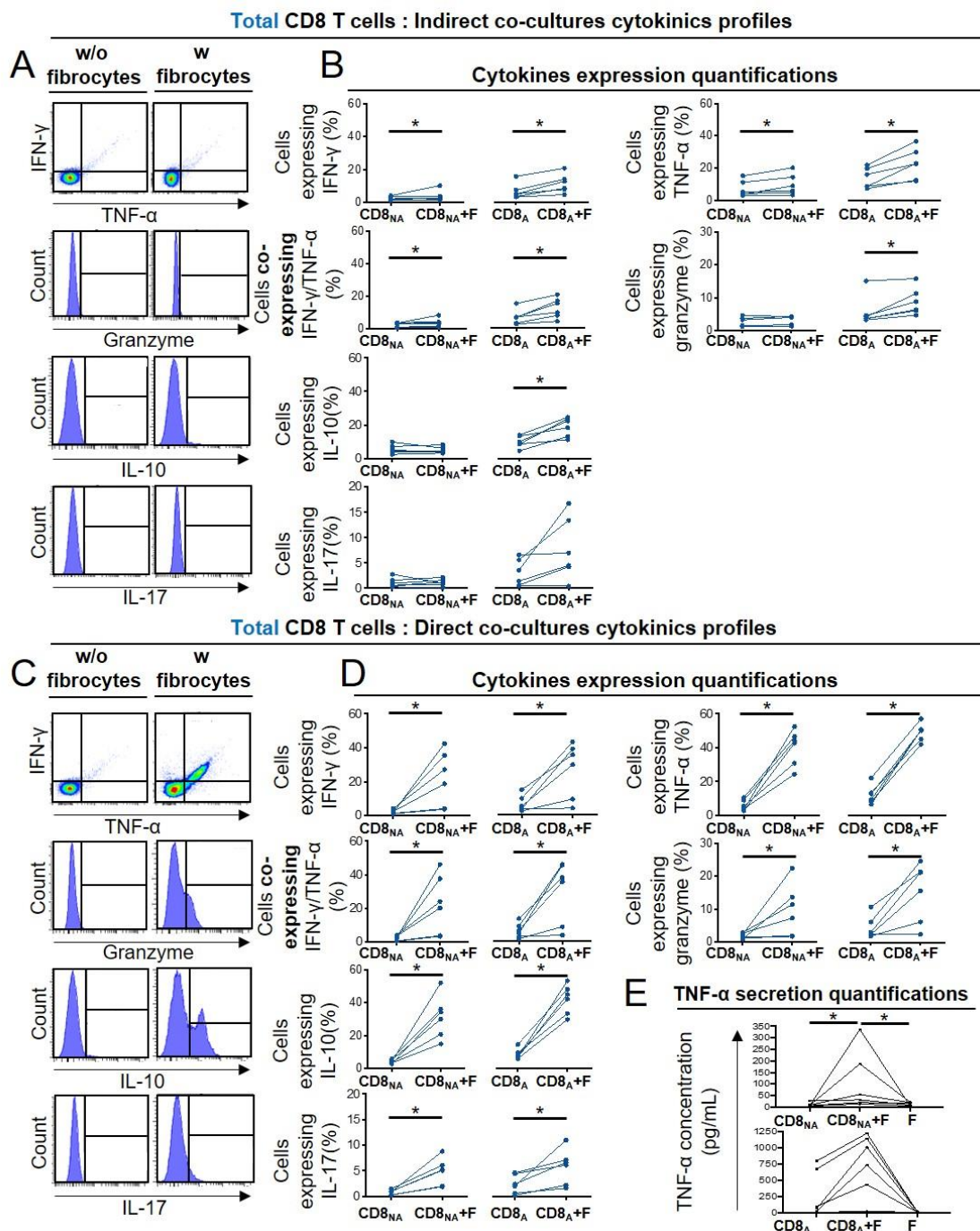


**Figure 5. Fibrocyte-CD8<sup>+</sup> T cell interactions alter cytokine production.** Prior to co-culture, CD8<sup>+</sup> T cells have been either non-activated (“CD8<sub>NA</sub>”) or activated (“CD8<sub>A</sub>”). (A, C) Representative gating strategy for identification of CD8<sup>+</sup> T cells expressing IFN- $\gamma$ , TNF- $\alpha$ , granzyme, IL-10 and IL17 without (w/o) fibrocytes (left panel) or with (w) fibrocytes (right panel) in indirect (A) or direct (C) co-culture. (B, D) Quantifications of CD8<sup>+</sup> T cells expressing IFN- $\gamma$ , TNF- $\alpha$ , both, granzyme and IL-10 after co-culture without fibrocytes (CD8<sub>NA</sub>/CD8<sub>A</sub>) or with fibrocytes (CD8<sub>NA</sub>/CD8<sub>A</sub>+F) in indirect (B) or direct (D) co-culture. (E) TNF- $\alpha$  concentrations in supernatants from co-cultures without fibrocytes (CD8<sub>NA</sub>/CD8<sub>A</sub>), with fibrocyte (CD8<sub>NA</sub>/CD8<sub>A</sub>+F), and only with fibrocytes (F) as control, for direct co-cultures. \* P < 0.05, Wilcoxon matched pairs test, Friedman test.

1327  
1328  
1329  
1330  
1331  
1332  
1333  
1334  
1335  
1336  
1337

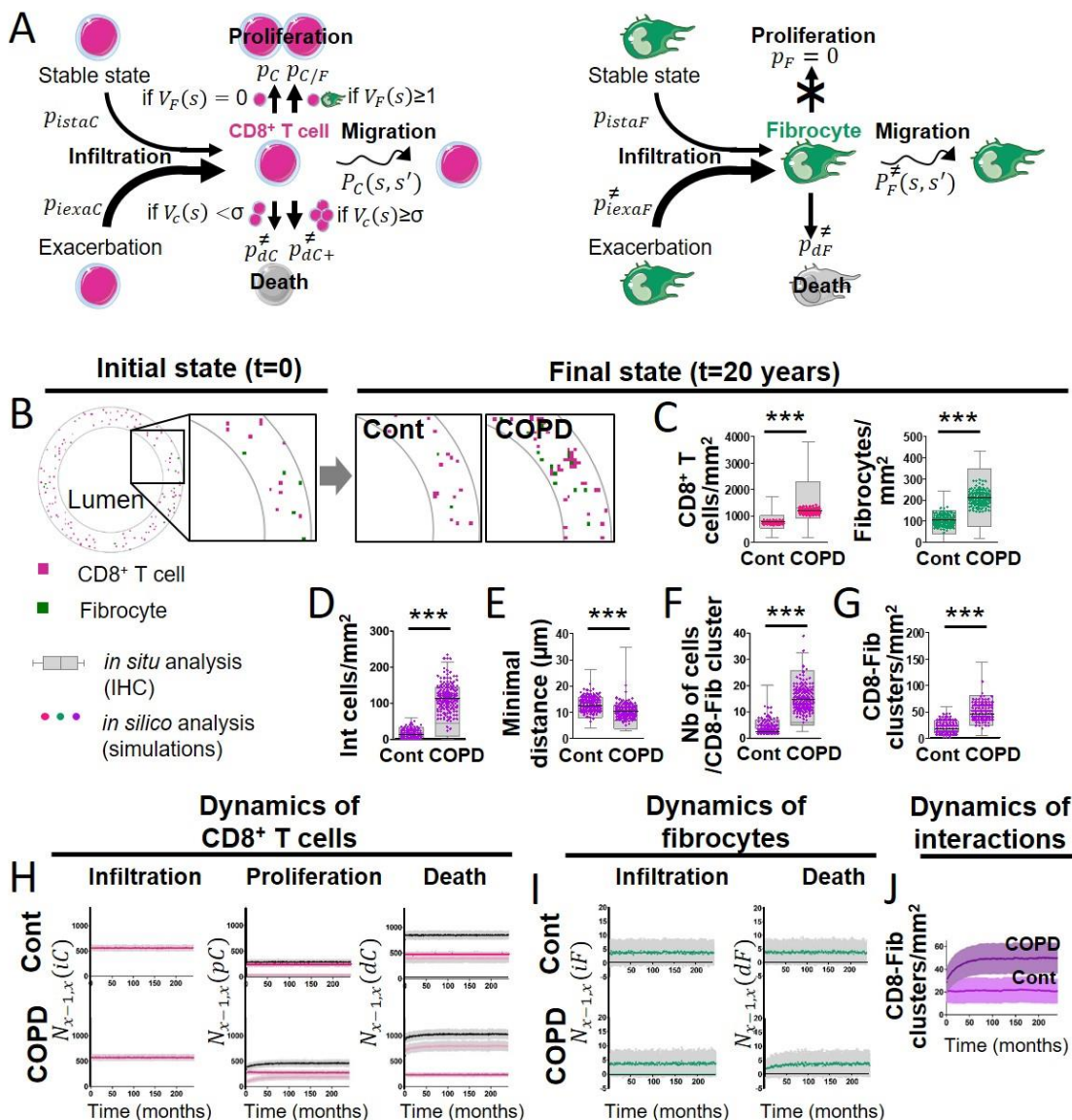


**Figure 6. A probabilistic cellular automata type model captures the features of the normal and pathological patterns of cell organisation observed in the tissues.** (A) Schematic representation of the probabilities associated with CD8<sup>+</sup> T cells (left panel) and fibrocytes (right panel). For each CD8<sup>+</sup> T cell, we define a "basal" probability  $p_{dC}$  of dying, an increased probability  $p_{dC+}$  of dying when the CD8<sup>+</sup> T cell has many other CD8<sup>+</sup> T cells in its neighbourhood, a "basal" probability  $p_C$  of dividing, an increased probability  $p_{C/F}$  of dividing when the CD8<sup>+</sup> T cell has fibrocytes in its neighbourhood, a probability  $P_C(s, s')$  of moving from a site  $s$  to a neighboring site  $s'$ , a probability  $p_{istaC}$  to be infiltrated at the stable state and a probability  $p_{iexaC}$  to be infiltrated during exacerbation. For each fibrocyte, we define a probability  $p_{dF}$  of dying, a probability  $p_F$  of dividing, a probability  $P_F(s, s')$  of moving from a site  $s$  to a neighboring site  $s'$ , a probability  $p_{istaF}$  to be infiltrated at the stable state and a probability  $p_{iexaF}$  to be infiltrated during exacerbation. The  $\neq$  symbol indicates parameters whose numerical value differs from control to COPD situation. (B) Selected representative pictures for initial state and final states after 20 years of control and COPD dynamics. Images surrounded by black squares: higher magnifications of peribronchial area. CD8<sup>+</sup> T cells and fibrocytes are represented respectively by pink and green squares. (C) CD8<sup>+</sup> T cells (left) and fibrocyte (right) densities. (D) Interacting cells densities of interacting cells. (E) Mean minimal distances between fibrocyte and CD8<sup>+</sup> T

1338  
1339  
1340  
1341  
1342  
1343  
1344  
1345  
1346  
1347  
1348  
1349  
1350  
1351  
1352  
1353  
1354  
1355  
1356

1357 cells. **(F)** CD8<sup>+</sup> T cells-fibrocytes-containing clusters (“CD8-Fib clusters”) densities. **(G)**  
1358 mean number of cells by CD8-Fib clusters. **(C-G)**, n=160 simulations for each situation.  
1359 The medians are represented as horizontal lines. The equivalent measurements measured on  
1360 patient’s tissues are represented by gray boxes (25<sup>th</sup> to the 75<sup>th</sup> percentile) and whiskers (min  
1361 to max). \*\*\*: P<0.001. unpaired t-tests or Mann-Whitney tests. **(H, I)** Mean kinetics of the  
1362 populations of CD8<sup>+</sup> T cells and fibrocytes in control and COPD situation *in silico*. Standard  
1363 deviations are indicated in gray, n=160 simulations. Left panels:  $N_{x-1,x}(iC)$  and  $N_{x-1,x}(iF)$   
1364 are the number of CD8<sup>+</sup> T cells (resp. fibrocytes) that have infiltrated the peribronchial area  
1365 for the month  $x$ , relatively to the surface of interest. For fibrocytes, the infiltration at the  
1366 stable state and during exacerbation are indicated respectively in green and light green. For  
1367 control situation, there is no infiltration by exacerbation. Middle panels:  $N_{x-1,x}(pC)$  is the  
1368 number of CD8<sup>+</sup> T cells that have proliferated for the month  $x$ , relatively to the surface of  
1369 interest. Basal duplication, fibrocyte-induced duplication and total duplication are indicated  
1370 respectively in pink, light pink and black. Right panels:  $N_{x-1,x}(dC)$  and  $N_{x-1,x}(dF)$  are the  
1371 number of CD8<sup>+</sup> T cells (resp. fibrocytes) that have died for the month  $x$ , relatively to the  
1372 surface of interest. For CD8<sup>+</sup> T cells, basal death, T cell-induced death and total death are  
1373 indicated respectively in pink, light pink and black. **(J)** Graphs showing the variations of  
1374 the mean densities of CD8-Fib clusters over time in control (light purple) and COPD  
1375 situation (dark purple).  
1376  
1377